Ceramics International

# Structural, Optical, Electrical, Dielectric, Molecular Vibrational and Magnetic Properties of La3+ doped Mg-Cd-Cu Ferrites Prepared by Co-precipitation Technique

--Manuscript Draft--

| | |
|---|---|
| **Manuscript Number:** | |
| **Article Type:** | Full length article |
| **Keywords:** | Co-precipitation; structural; magnetic; electric; dielectric; optical |
| **Corresponding Author:** | Nguyễn Thi Kim Thanh, PhD<br>University College London<br>London, UNITED KINGDOM |
| **First Author:** | Muhammad Imran Arshad |
| **Order of Authors:** | Muhammad Imran Arshad |
| | Atta Ur Rehman |
| | M. S. Hasan |
| | Maria Akhtar |
| | Le Duc Tung |
| | Nasir Amin |
| | Dr. Khalid Mahmood |
| | Thithawat Trakoolwilaiwan |
| | Nguyễn Thi Kim Thanh, PhD |
| **Abstract:** | Ferrites are among the most frequently investigated materials mainly due to interesting and practically different properties. Therefore, easily and cost-effective lanthanum doped Mg 0.5 Cd 0.25 Cu 0.25 Fe 2-x La x O 4 (x = 0.0, 0.0125, 0.025, 0.0375 and 0.05) ferrites were synthesized by a co-precipitation route, a comprehensive characterisation of their structural, optical, electric, dielectric, molecular vibrational, and magnetic properties were carried out. X-ray diffraction analysis confirmed the formation of a cubic spinel structure. Variations in frequency bands were also observed with amplification in optical band gap energy (2.95 – 3.38 eV) due to La 3+ ions insertion. The electric resistivity had opposite trends at low and high temperatures with increasing La 3+ content. The Curie temperature, activation energy, and drift mobility were also determined to have values consistent with the semiconducting behavior of the soft ferrites. The saturation magnetization (M S ) has a maximum value 49.385 emu/g with remanent magnetization (M r ) was 34.9283 emu/g and coercivity 661.4 Oe for La 3+ concentration x = 0.05. The minimum dielectric loss was observed for La 3+ concentration x = 0.025. Moreover, the resistivity (ρ) has a maximum value of 7.95 × 10 4 Ω cm for La 3+ concentration x = 0.025. The calculated frequency range of La 3+ doped Mg-Cd-Cu ferrites was detected in the microwave range (3.36 – 10.80 GHz), suggesting the potential application of the materials in longitudinal recording media and microwave absorbance. |
| **Suggested Reviewers:** | Dr, Niroj Kumar Sahu, Ph.D<br>Associate Professor, Vellore Institute of Technology: VIT University<br>nirojs@vit.ac.in |
| | Prof. Nicola a Morley, Ph.D<br>Prof<br>n.a.morley@sheffield.ac.uk |
| | Muhammad Tariq Sajjad<br>sajjadt@lsbu.ac.uk |
| **Opposed Reviewers:** | |

# Structural, Optical, Electrical, Dielectric, Molecular Vibrational and Magnetic Properties of $La^{3+}$ doped Mg-Cd-Cu Ferrites Prepared by Co-precipitation Technique

Muhammad Imran Arshad[a*], Atta Ur Rehman[a], M. S. Hasan[b], Maria Akhtar[a], Le Duc Tung[c,d], N. Amin[a], Khalid Mahmood[a], Thithawat Trakoolwilaiwan[c,d,e], and Nguyen Thi Kim Thanh[c,d**].

[a]Department of Physics, Government College University, Faisalabad 38000, Pakistan.

[b]Department of Physics, University of Lahore, 1-kM Raiwind Road, Lahore, 54000, Pakistan.

[c]Biophysics Group, Department of Physics and Astronomy, University College London, Gower Street, London, WC1E 6BT, UK.

[d]UCL Healthcare Biomagnetic and Nanomaterials Laboratories, 21 Albemarle Street, London W1S 4BS, UK

[e]Healthy Infrastrcture Research Group, University College London, WC1E 6BT, UK

Corresponding author: [*]miarshadgcuf@gmail.com; [**]ntk.thanh@ucl.ac.uk

## Abstract

Ferrites are among the most frequently investigated materials mainly due to interesting and practically different properties. Therefore, easily and cost-effective lanthanum doped $Mg_{0.5}Cd_{0.25}Cu_{0.25}Fe_{2-x}La_xO_4$ (x = 0.0, 0.0125, 0.025, 0.0375 and 0.05) ferrites were synthesized by a co-precipitation route, a comprehensive characterisation of their structural, optical, electric, dielectric, molecular vibrational, and magnetic properties were carried out. X-ray diffraction analysis confirmed the formation of a cubic spinel structure. Variations in frequency bands were also observed with amplification in optical band gap energy (2.95 – 3.38 eV) due to $La^{3+}$ ions insertion. The electric resistivity had opposite trends at low and high temperatures with increasing $La^{3+}$ content. The Curie temperature, activation energy, and drift mobility were also determined to have values consistent with the semiconducting behavior of the soft ferrites. The saturation magnetization ($M_S$) has a maximum value 49.385 emu/g with remanent magnetization ($M_r$) was 34.9283 emu/g and coercivity 661.4 Oe for $La^{3+}$ concentration x = 0.05. The minimum dielectric loss was observed for $La^{3+}$ concentration x = 0.025. Moreover, the resistivity (ρ) has a maximum value of $7.95 \times 10^4$ Ω cm for $La^{3+}$ concentration x = 0.025. The calculated frequency range of $La^{3+}$ doped Mg-Cd-Cu ferrites was detected in the microwave range (3.36 – 10.80 GHz), suggesting the potential application of the materials in longitudinal recording media and microwave absorbance.

**Keywords:** Co-precipitation; structural; magnetic; electric; dielectric; optical.

## Graphical Abstract

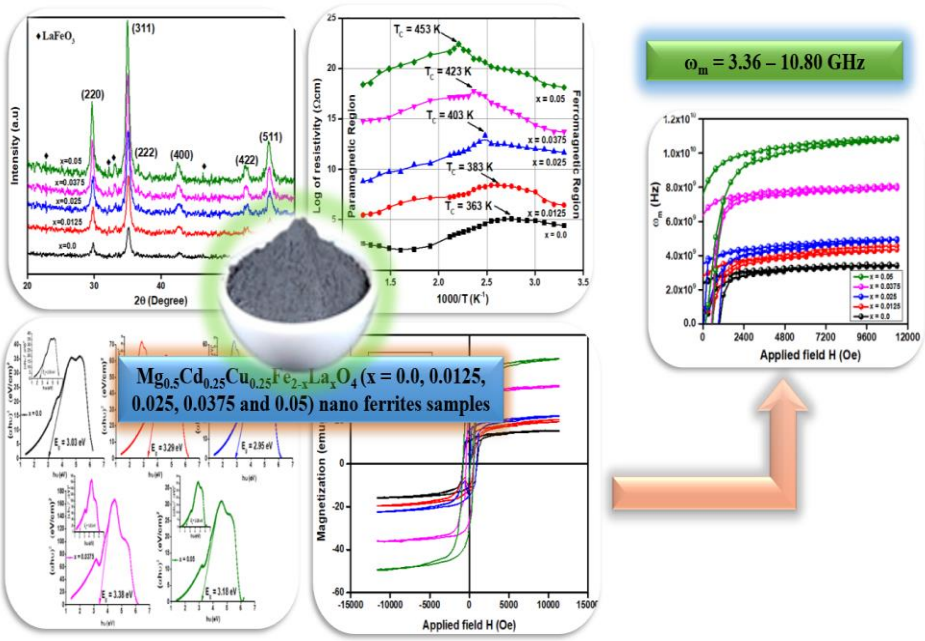


## Highlights

- $La^{3+}$ doped Mg-Cd-Cu ferrites samples synthesized *via* co-precipitation.
- The lattice constant increased with $La^{3+}$ substitution.
- At 303 K, for $La^{3+}$ concentration x = 0.025, maximum resistivity was observed.
- Magnetization saturation was increased with $La^{3+}$ concentration.

## 1. Introduction

Soft spinel ferrites $AFe_2O_4$ (A = metal ions) have played an active role in the development of science and technology with potential applications in medical, storage devices, electric, electronics, optoelectronics, microwave, and electromagnetic devices [1-7]. For the synthesis of soft spinel ferrites particles, there have been several methods including spray pyrolysis [8], citrate gel [9-11], hydrothermal [12], microwave refluxing [13], and co-precipitation [14-18]. Co-precipitation is one of the common and low price synthesis techniques with vast potentials [19] of which the microstructural, optical, electric, dielectric, and magnetic properties of the materials can be controlled by the synthetic process. Also, Co-precipitation is one of the most effective methods for controlling crystallite size and other material characteristics [20].

In spinel ferrites $AFe_2O_4$, the electric and magnetic properties can be changed by the locations of different metal ions A on tetrahedral or octahedral sites as well as changes in chemical compositions [9, 10, 12, 13]. In sonochemical synthesized $CuFe_{1.85}La_{0.15}O_4$ ferrite, it was reported a reduction in saturation magnetization and a rise in coercivity as compared with $CuFe_2O_4$ [21]. The influence of $La^{3+}$ on $(Cu\text{-}Cd)Fe_{2-x}La_xO_4$ soft ferrites was investigated, where it was seen a decrease in saturation magnetization with the addition of dopant $La^{3+}$ [22]. The incorporation of $La^{3+}$ in the $MgFeO_4$ ferrite can improve the magnetic parameters to be useful for microwave applications. $La^{3+}$ doped $MgLa_xFe_{2-x}O_4$ ferrites fabricated by sol-gel process were reported a potential candidate for microwave absorption applications of which the saturation magnetization was observed to increase from 12.51 emu/g (for x = 0.0) to 19.39 emu/g (for x = 0.05) [23]. Patil *et al*., [24] reported that the intensity of peaks reduces with substitution of $La^{3+}$ up to $x = 0.025$ and then increases for $x = 0.035$. It indicates that at lower concentrations the $La^{3+}$ ions substituted completely in the spinel lattice having compositions $x \leq 0.025$. On the other hand, at higher concentrations ($x = 0.035$), the $La^{3+}$ ions are less substituted in the spinel lattice. Therefore, the $LaFeO_3$ phase was developed at the grain boundaries due to unsubstituted $La^{3+}$ ions. Chaudhary *et al*. [25] reported that in Ni–Cu–Zn ferrites the maximum limit for replacement of $Fe^{3+}$ by $La^{3+}$ are up to $x = 0.025$. Zhou *et al*., [26] also reported that the maximum limit of the substitution of $La^{3+}$ is $x$ = 0.02 then the $LaFeO_3$ phase appeared. Rehman *et al*., (2021) [27] reported $Zn_{0.5}Co_{0.25}Cu_{0.25}La_{0.125}Fe_{1.875}O_4$ ferrite and observed the $LaFeO_3$ phase at 33°. Asma *et al*., [28] observed that the intensity of $LaFeO_3$ phase in $La^{3+}$ doped Mg-Ni-Co-Cu ferrites was increased for $La^{3+}$ concentration $x$ = 0.06 to $x$ = 0.15. Rehman *et al*., (2020) [29] also report $La^{3+}$ doped Zn-Co-Cu ferrites and

observed the additional peak of $LaFeO_3$ phase at 33° from $La^{3+}$ concentration $x$ = 0.0125 to $x$ = 0.05. Gadkari *et al.*, [30] reported Mg-Cd ferrites with the addition of $La^{3+}$ ions prepared *via* the co-precipitation method. Pure Mg–Cd ferrites have a smaller saturation magnetization as compared to $La^{3+}$ added Mg-Cd ferrite. This can be due to the higher density and structural and chemical uniformity achieved by chemically preparing ferrite. With the addition of $La^{3+}$, the saturation magnetization, coercivity, and remnant magnetization all increased and these findings were encouraging for high-frequency applications. For microwave frequency applications, it is desirable to have high saturation magnetization. Microwave operating frequency was determined using relation $\omega_m = 8\pi^2 M_s \gamma$, where γ is a gyromagnetic fraction with the significance of 2.8 MHz/Oe [23, 27, 31, 32]. The larger the saturation magnetization, the greater will be the microwave operating frequency. According to the literature, the addition of $La^{3+}$ in the $CuFeO_4$ and Cu-Cd ferrites reduced the saturation magnetization. On the other hand, the substitution of $La^{3+}$ in $MgFeO_4$ and Mg-Cd ferrites enhanced saturation magnetization. Therefore, the literature study motivates for deeper analysis of the impact of $La^{3+}$ on the Mg-Cd-Cu ferrites.

In current work, we examine the impact of $La^{3+}$ doping in Mg-Cd-Cu ferrites (x = 0, 0.0125, 0.025, 0.0375 and 0.05) prepared *via* co-precipitation route. We have examined the structural, optical, electric, vibrational, dielectric, and magnetic properties to employ the materials for commercial usages.

## 2. Synthesis of $La^{3+}$ doped Mg-Cd-Cu samples

$Mg(NO_3)_2.6H_2O$, $Cd(NO_3)_2.4H_2O$, $Cu(NO_3)_2.3H_2O$, $Fe(NO_3)_3.9H_2O$, and $La(NO_3)_3.9H_2O$ salts from Sigma Aldrich with 99.99 % purity were used to fabricate $Mg_{0.5}Cd_{0.25}Cu_{0.25}Fe_{2-x}La_xO_4$ (x = 0.0, 0.0125, 0.025, 0.0375 and 0.05). x is predicted based on the precursor stoichiometric fractions (Table 1). The salts with stoichiometric fractions were dissolved in deionized water having mixed solution pH 2 and placed on a hot plate at 60 °C with magnetic stirring. Caustic soda solution was prepared with the combination of 12 g NaOH in 100 mL deionized water to maintain the solution with pH 12. The mixed solution of the precursor was kept in an 80 °C preheated water bath for 24 h to complete the ionization of metal nitrates. The precipitates were cleaned with ethanol and deionized water several times and filtered with Whatman papers to eliminate impurities and then dehydrate in the oven at 80 °C. After that the sintering was performed in a muffle furnace at 850 °C at the rate of 5 °C/min for 8 h. Sintering is the process of compacting powders at high temperatures below melting point until a change in microstructure occurs, including grain growth, higher density or shrinkage, pore

reduction [33]. Then the obtained materials were ground into fine crystal powder. The whole process of the experiment is shown in Fig. 1.

**Table 1 Stoichiometric Calculations of all the compounds used**

| x | Mg $(NO_3)_2.6H_2O$ | Cd $(NO_3)_2.4H_2O$ | Cu $(NO_3)_2.3H_2O$ | Fe $(NO_3)_3.9H_2O$ | La $(NO_3)_3.6H_2O$ |
|---|---|---|---|---|---|
| 0.0 | 128.2 mg/ mL | 177.1 mg/ mL | 46.89 mg/ mL | 806.00 mg/ mL | 0.0 mg/ mL |
| 0.0125 | 128.2 mg/ mL | 177.1 mg/ mL | 46.89 mg/ mL | 802.95 mg/ mL | 4.06 mg/ mL |
| 0.025 | 128.2 mg/ mL | 177.1 mg/ mL | 46.89 mg/ mL | 797.90 mg/ mL | 8.12 mg/ mL |
| 0.0375 | 128.2 mg/ mL | 177.1 mg/ mL | 46.89 mg/ mL | 792.85 mg/ mL | 12.18 mg/ mL |
| 0.05 | 128.2 mg/ mL | 177.1 mg/ mL | 46.89 mg/ mL | 787.80 mg/ mL | 16.20 mg/ mL |

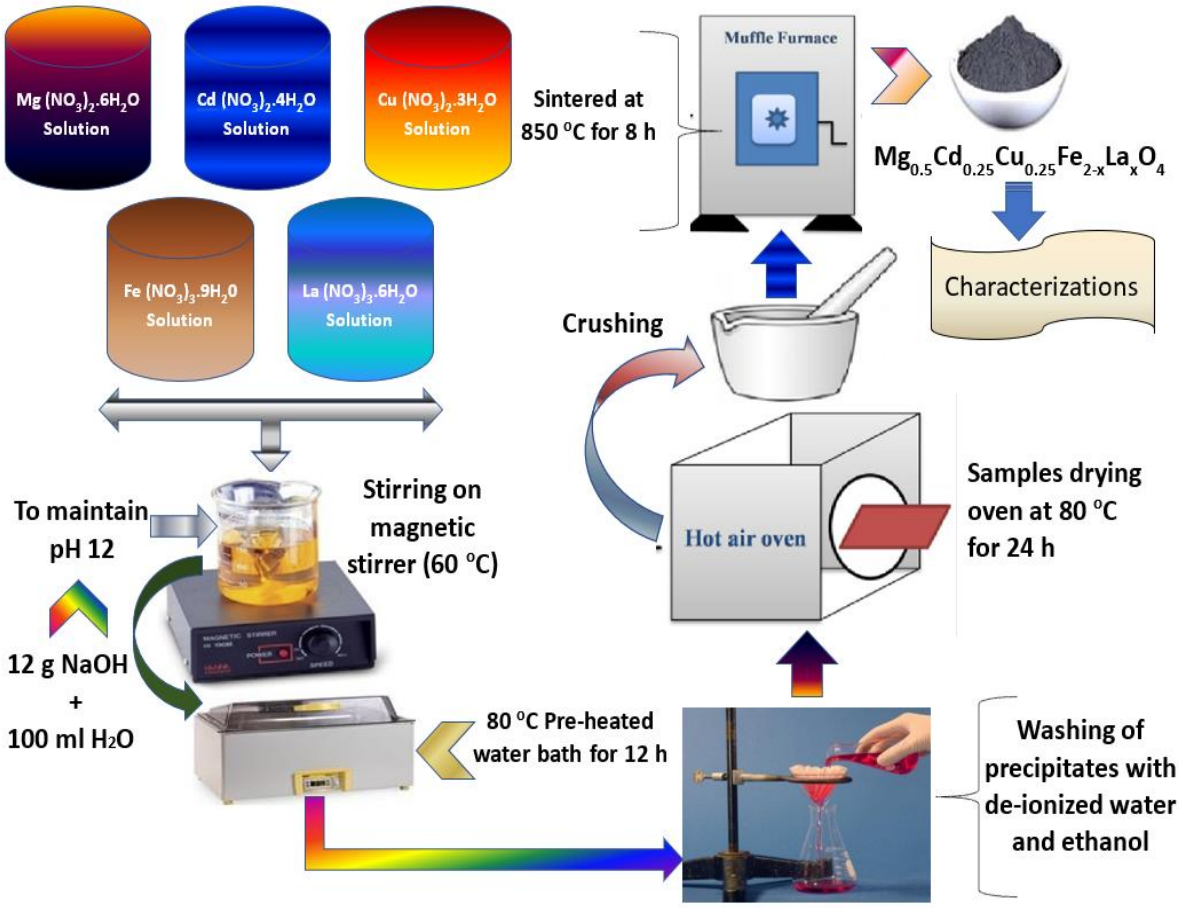


**Fig. 1** Schematic diagram for the synthesis of $La^{3+}$ doped Mg-Cd-Cu soft ferrite samples

The crystallographic structure of the soft ferrites is investigated using XRD and Rietveld refinement performed using FullProf software. The Fourier transformation infrared spectroscopy (FTIR) was utilized to reveal absorption bands and force constant. Perkin Elmer, Model Lambda 25, UV-Visible Double Beam Spectrophotometer (UV-DS) was used to determine the optical bandgap of the as-prepared sample. It offered an easy way to analyze the

different features such as energy bandgap and ion transition from lower to higher energy levels. The electric properties were studied using two probes connected with Keithley 2401 Source Meter. The dielectric behavior was measured *via* an IM3536 LCR meter. The magnetic behavior was studied using VSM 7400, at 303 K.

## 3. Experimental Results and Discussion

### 3.1 Structural Study

XRD patterns of $La^{3+}$ doped Mg-Cd-Cu ferrites are given in Fig. 2. Various peaks were detected with Miller indices (hkl) = (220), (311), (222), (400), (422), (511) corresponding to the structure of the spinel ferrites and secondary phase $LaFeO_3$ [29]. The XRD peaks confirm $La^{3+}$ being successfully doped into the spinel structure. From the XRD patterns, the lattice constant (a) and crystallite size (D) were derived, and the values are given in Table 2. It can be seen from Fig. 3 that the nonlinear relationship between the crystallite size (D) as well as the lattice parameter (a) on the lanthanum content. From the XRD pattern, the X-ray density ($d_x$) and bulk density ($d_b$) were determined using $d_b = M/\pi r^2 h$, where 'M' indicates the mass of the pellets while 'h' and 'r' represent the thickness and radius of the pellet, respectively [34-36], and given in Table 2. It was observed that the bulk density ($d_b$) rises with increasing La doping being consistent with the fact that $La^{3+}$ has an atomic weight of 138.905, much higher than 55.845 of $Fe^{3+}$. From Table 2 it is clear that the "$d_x$" is larger than the "$d_b$" for all the as-prepared samples, which might be due to the presence of unavoidable pores during the process of sintering [37].

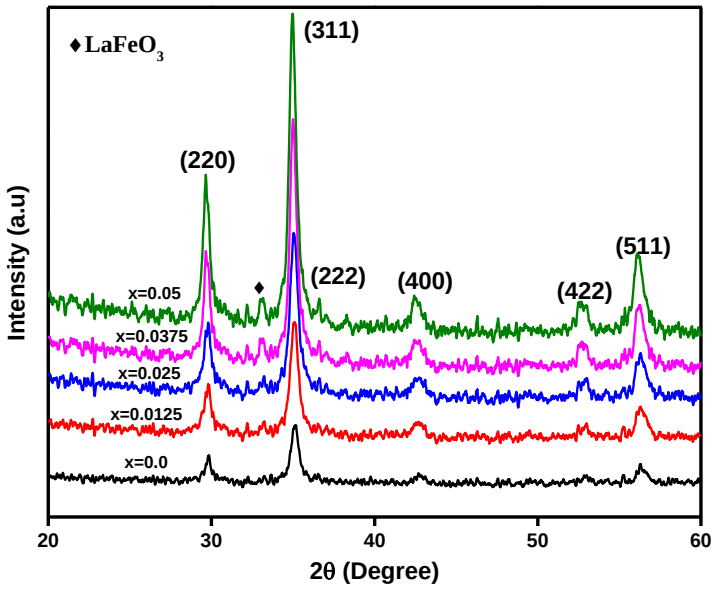


**Fig. 2** XRD pattern for $La^{3+}$ doped Mg-Cd-Cu ferrite samples

**Table 2** Structural parameters for $La^{3+}$ doped Mg-Cd-Cu ferrites samples

| Parameters | Concentration (x) | | | | |
|---|---|---|---|---|---|
| | **0.00** | **0.0125** | **0.025** | **0.0375** | **0.05** |
| **2θ (311) peak** | 35.06 | 34.99 | 35.02 | 34.96 | 34.85 |
| **d (Å)** | 2.56 | 2.56 | 2.57 | 2.57 | 2.58 |
| **a (Å)** | 8.50 | 8.49 | 8.51 | 8.52 | 8.54 |
| **D (nm)** | 26.5 | 29.4 | 32.2 | 25.3 | 26.0 |
| **V $(Å)^3$** | 614.12 | 613.69 | 616.29 | 619.34 | 624.14 |
| **$d_X$ $(gcm^{-3})$** | 5.01 | 5.03 | 5.04 | 5.04 | 5.02 |
| **$d_b$ $(gcm^{-3})$** | 3.91 | 3.93 | 3.95 | 3.97 | 3.99 |

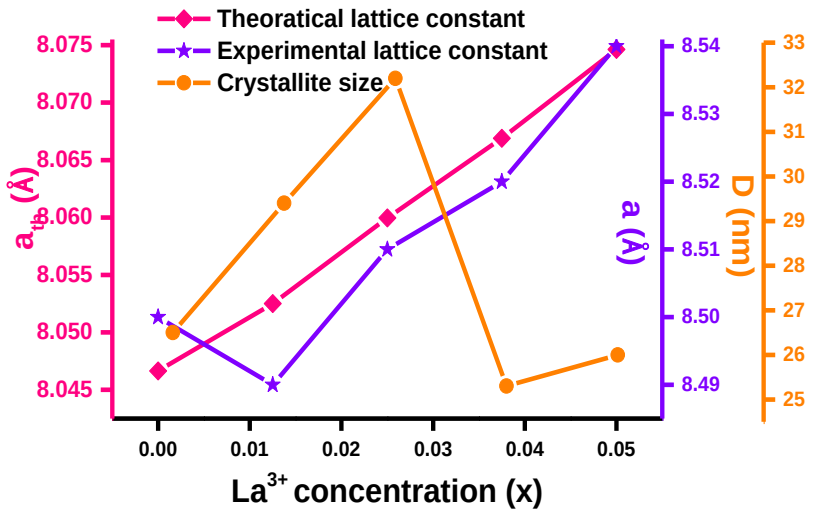


**Fig. 3** The graphical representation of theoretical and experimental lattice constant

Fig. 4 shows the XRD patterns refined using the Rietveld refinement method for $La^{3+}$ doped Mg-Cd-Cu ferrites. The space group of ferrite systems belonging to *F d* -3 *m* was revealed by the Rietveld refinement. The exitances of the $LaFeO_3$ phase are also reported in the literature [29, 38]. The R-factors including, the Bragg factor ($R_{Bragg}$), expected factor ($R_{exp}$), weighted profile factor ($R_{wp}$), profile factor ($R_p$), and goodness-of-fit ($\chi^2$) are all used to determine the refinement's reliability (are listed in Table 3). With the inclusion of $La^{3+}$ ions into the Mg-Cd-Cu ferrite, the lattice constant ($a_{rv}$) determined *via* the Rietveld refinement method was increased from 8.4617 to 8.5198 Å. The unit cell volume (V) was also increased from 605.86 to 618.43 $(Å)^3$ as the substitution of $La^{3+}$ increased. A similar increasing trend was reported by Aslam *et al.* [38]. It was found from Table 3 that the crystallite size was reduced from 13.88 to 12.59 nm with the substitution of $La^{3+}$ change from x = 0.0 to x = 0.05. It may be due to a stronger La–O bond as compared to Fe–O [38]. This means that high energy is needed for the substitution of $La^{3+}$ at the octahedral site in Mg-Cd-Cu ferrite as reported by

Aslam *et al.*, [38]. The strain (ε) was increased with the addition of $La^{3+}$ in the spinel lattice (as seen in Table 3).

**Table 3** R-Factors, goodness-of-fit (GoF), and lattice constants determined by Rietveld refinement ($a_{rv}$) methods for $La^{3+}$ doped Mg-Cd-Cu ferrites samples

| x | R-Factors | | | | | GoF | Lattice Parameters | | | |
|---|---|---|---|---|---|---|---|---|---|---|
| | $R_p$ | $R_{wp}$ | $R_{exp}$ | $R_{Bragg}$ | $R_F$ | $\chi^2$ | $a_{rv}$ (Å) | V $(Å)^3$ | D (nm) | ε |
| 0.0 | 14.5 | 10.8 | 9.63 | 2.642 | 2.703 | 1.12 | 8.4617 | 605.86 | 13.88 | 0.00864 |
| 0.0125 | 15.6 | 9.78 | 9.30 | 2.759 | 2.687 | 1.05 | 8.4773 | 609.23 | 13.74 | 0.00874 |
| 0.025 | 13.5 | 9.39 | 8.54 | 2.872 | 2.864 | 1.09 | 8.4826 | 610.38 | 13.30 | 0.00903 |
| 0.0375 | 15.3 | 9.34 | 9.12 | 2.275 | 2.549 | 1.02 | 8.4998 | 614.09 | 13.24 | 0.00909 |
| 0.05 | 12.5 | 9.99 | 8.93 | 2.698 | 2.961 | 1.11 | 8.5198 | 618.43 | 12.59 | 0.00959 |

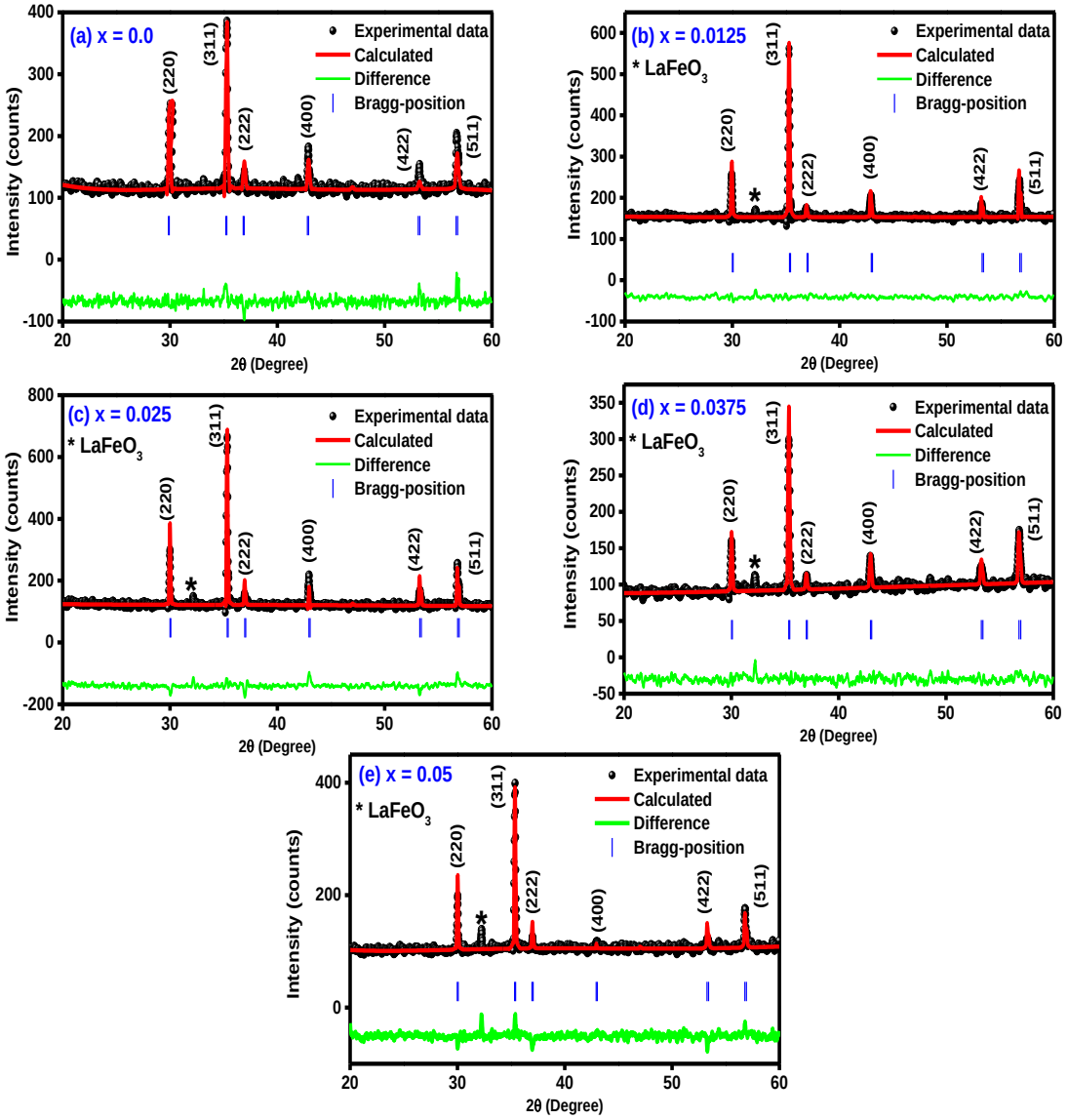


**Fig. 4** XRD patterns using Rietveld refinement

$Cd^{2+}$ ferrites have a normal spinel structure and occupancy only into the tetrahedral (A) site [39]. The occupancy of $Mg^{2+}$, $Fe^{3+}$, and $La^{3+}$ ions into the tetrahedral and octahedral sites [39]. The cations distribution of $La^{3+}$ substituted Mg-Cd-Cu ferrites are given in Table 4. This cations distribution is based on the following hypotheses: (1) At the tetrahedral site, the sum of cation distribution is one, and at the octahedral site, it is two. (2) The net charge of the spinel ferrite must be zero. As a result, to create an electrically neutral crystal matrix, the number of positive charges in the compound is equal to the negative charges [39]. It can be observed that tetrahedral radii ($r_A$) remain constant because there is no change in the distribution of cations at the tetrahedral site, and octahedral radii ($r_B$) is increased with the substitution of dopant ion (Table 4). The extension in "$r_B$" is due to higher ionic radii $La^{3+}$ (1.06 Å) as compared to the cationic radii of $Fe^{3+}$ (0.64 Å). By utilizing the calculated results of "$r_A$" and "$r_B$" radii at different lattice sites, the theoretical lattice constant ($a_{th}$) [17] is determined and is reported in Table 4. The graphically both theoretical lattice constant ($a_{th}$) and the experimental lattice constant (a) *versus* $La^{3+}$ concentration (x) as shown in Fig.3. The theoretical lattice constant ($a_{th}$) is slightly smaller than the experimental lattice constant (a) may be due to the difference in ionic radii and an account of the supposition of cations and anions normal arrangements in perfect unit cell structure obtained for theoretical computations [40].

**Table 4** Cationic distribution at sub-lattice A and B sites, tetrahedral and octahedral ionic radii ($r_A$ and $r_B$), the theoretical lattice constant ($a_{th}$)

| x | Tetrahedral (A) site | Octahedral (B) site | $r_A$ (Å) | $r_B$ (Å) | $a_{th}$ (Å) |
|---|---|---|---|---|---|
| 0.0 | $Mg_{0.225}Cd_{0.25}Cu_{0.025}Fe_{0.5}$ | $Mg_{0.275}Cu_{0.225}Fe_{1.5}$ | 0.4685 | 0.6649 | 8.0466 |
| 0.0125 | $Mg_{0.225}Cd_{0.25}Cu_{0.025}Fe_{0.5}$ | $Mg_{0.275}Cu_{0.225}Fe_{1.4875}La_{0.0125}$ | 0.4685 | 0.6671 | 8.0525 |
| 0.025 | $Mg_{0.225}Cd_{0.25}Cu_{0.025}Fe_{0.5}$ | $Mg_{0.275}Cu_{0.225}Fe_{1.475}La_{0.025}$ | 0.4685 | 0.6699 | 8.0599 |
| 0.0375 | $Mg_{0.225}Cd_{0.25}Cu_{0.025}Fe_{0.5}$ | $Mg_{0.275}Cu_{0.225}Fe_{1.4625}La_{0.0375}$ | 0.4685 | 0.6725 | 8.0669 |
| 0.05 | $Mg_{0.225}Cd_{0.25}Cu_{0.025}Fe_{0.5}$ | $Mg_{0.275}Cu_{0.225}Fe_{1.45}La_{0.05}$ | 0.4685 | 0.6754 | 8.0746 |

The smallest distance at A-site cations and $O^{2-}$ ions are known as bond length ($R_A$), and the shortest distance at B-site cations and $O^{2-}$ ions are known as bond length ($R_B$) [17]. The values of bond length ($R_A$) and bond length ($R_B$) were determined from Rietveld refinement and the theoretical bond length ($R'_A$) and bond length ($R'_B$) were also determined [17]. It is clear from Table 5 that the bond length "$R_A$" is increased, and "$R_B$" is also increased with the increment of dopant cations. The values of "$R'_A$" and "$R'_B$" is larger than "$R_A$" and "$R_B$", respectively. The increasing values of "$R'_B$" suggests that $La^{3+}$ are spread across octahedral (B) site in the spinel structure.

The interatomic distances involve $d_{AL}$, $d_{BL}$, and $d_{BLU}$ represents tetrahedral edge length, shared octahedral edge length, and unshared octahedral edge length. The calculated values are

given in Table 5. Magnetic properties of spinel ferrites depend on the exchange interactions as well as on the interionic lengths and bond angles amongst the metal ions. Magnetic interaction A–B, A–A and B–B are related to bond length and bond angles among cations–cations and cations– anions. Further, it has been observed that bond angles have direct relations with the strength of magnetic exchange interactions. In contrast, interionic lengths have an inverse relationship with the strength of magnetic exchange interactions [41]. The cations–anions (Me–O) and cations–cations (Me–Me) interionic distances along with bond angles were calculated using relations as given in Table 6. The values of interionic distances are reported in Table 7. Bond angles were also calculated with the help of cations-cation and cations-anions interionic distance for all the as-prepared ferrites [42]. It can be seen from Table 8 that with increasing the concentration of $La^{3+}$, the bond angles $\theta_1$, $\theta_2$, and $\theta_5$ increased and indicates stronger (A–B) and (A–A) interaction. The decrease in $\theta_2$ and $\theta_4$ bond angles show weaker (B–B) interaction with the doping of $La^{3+}$ cations [43]. The relation between interionic distance and bond angles is shown in Fig.5.

**Table 5** Bond lengths ($R_A$, $R_B$, $R'_A$, $R'_B$), Bond edge lengths ($d_{AL}$, $d_{BL}$, and $d_{BLU}$) for $La^{3+}$ doped Mg-Cd-Cu ferrites

| x | Bond lengths (Å) | | | | Bond edge lengths (Å) | | |
|---|---|---|---|---|---|---|---|
| | $R_A$ | $R_B$ | $R'_A$ | $R'_B$ | $d_{AL}$ | $d_{BL}$ | $d_{BLU}$ |
| 0.0 | 1.9439 | 2.0508 | 1.8892 | 2.0967 | 3.0851 | 2.9252 | 3.0057 |
| 0.0125 | 1.9459 | 2.0555 | 1.8856 | 2.0950 | 3.0792 | 2.9240 | 3.0021 |
| 0.025 | 1.9455 | 2.0577 | 1.8883 | 2.1010 | 3.0836 | 2.9338 | 3.0092 |
| 0.0375 | 1.9479 | 2.0627 | 1.8889 | 2.1044 | 3.0846 | 2.9399 | 3.0127 |
| 0.05 | 1.9508 | 2.0685 | 1.8915 | 2.1104 | 3.0889 | 2.9497 | 3.0197 |

**Table 6** Relation used to find out the interionic distances and bond angles

| Cation-Anion | Cation-Cation | Bond angles |
|---|---|---|
| $p = \left(\frac{5}{8} - u\right)a$ | $b = \sqrt{2}\left(\frac{a}{4}\right)$ | $\theta_1 = \left(\frac{p^2 + q^2 - c^2}{2pq}\right)$ |
| $q = \left(U - \frac{1}{4}\right)\sqrt{3}a$ | $c = \sqrt{11}\left(\frac{a}{8}\right)$ | $\theta_2 = \left(\frac{p^2 + r^2 - e^2}{2pr}\right)$ |
| $r = \left(u - \frac{1}{4}\right)\sqrt{11}a$ | $d = \sqrt{3}\left(\frac{a}{4}\right)$ | $\theta_3 = \left(\frac{2p^2 - b^2}{2p^2}\right)$ |
| $s = \left(\frac{1}{3}u + \frac{1}{8}\right)\sqrt{3}a$ | $e = \sqrt{3}\left(\frac{3a}{8}\right)$ | $\theta_4 = \left(\frac{p^2 + s^2 - f^2}{2ps}\right)$ |
| | $f = \sqrt{6}\left(\frac{a}{4}\right)$ | $\theta_5 = \left(\frac{r^2 + q^2 - d^2}{2rq}\right)$ |

**Table 7** Values of interionic lengths among cations – cations (Me – Me) and cations – anions (Me – O) of soft ferrites

| x | Cation – Anion (Me – O) | | | Cation – Cation (Me – Me) | | | | | |
|---|---|---|---|---|---|---|---|---|---|
| | p (Å) | q (Å) | r (Å) | s (Å) | b (Å) | c (Å) | d (Å) | e (Å) | f (Å) |
| 0.0 | 2.0967 | 1.8892 | 3.6176 | 3.6969 | 3.0052 | 3.5239 | 3.6806 | 5.5209 | 5.2051 |
| 0.0125 | 2.0950 | 1.8856 | 3.6107 | 3.6921 | 3.0016 | 3.5197 | 3.6762 | 5.5144 | 5.1990 |
| 0.025 | 2.1010 | 1.8883 | 3.6159 | 3.7002 | 3.0087 | 3.5280 | 3.6849 | 5.5274 | 5.2112 |
| 0.0375 | 2.1044 | 1.8889 | 3.6170 | 3.7040 | 3.0122 | 3.5322 | 3.6892 | 5.5339 | 5.2174 |
| 0.05 | 2.1104 | 1.8915 | 3.6220 | 3.7121 | 3.0193 | 3.5405 | 3.6979 | 5.5468 | 5.2296 |

**Table 8** Bond angles for $La^{3+}$ doped Mg-Cd-Cu ferrites soft ferrites

| x | $\theta_1$ | $\theta_2$ | $\theta_3$ | $\theta_4$ | $\theta_5$ |
|---|---|---|---|---|---|
| 0.0 | 124.19 | 148.94 | 91.55 | 125.62 | 76.84 |
| 0.0125 | 124.22 | 149.09 | 91.51 | 125.61 | 76.93 |
| 0.025 | 124.26 | 149.28 | 91.45 | 125.60 | 77.04 |
| 0.0375 | 124.29 | 149.46 | 91.40 | 125.58 | 77.14 |
| 0.05 | 124.33 | 149.66 | 91.34 | 125.57 | 77.25 |

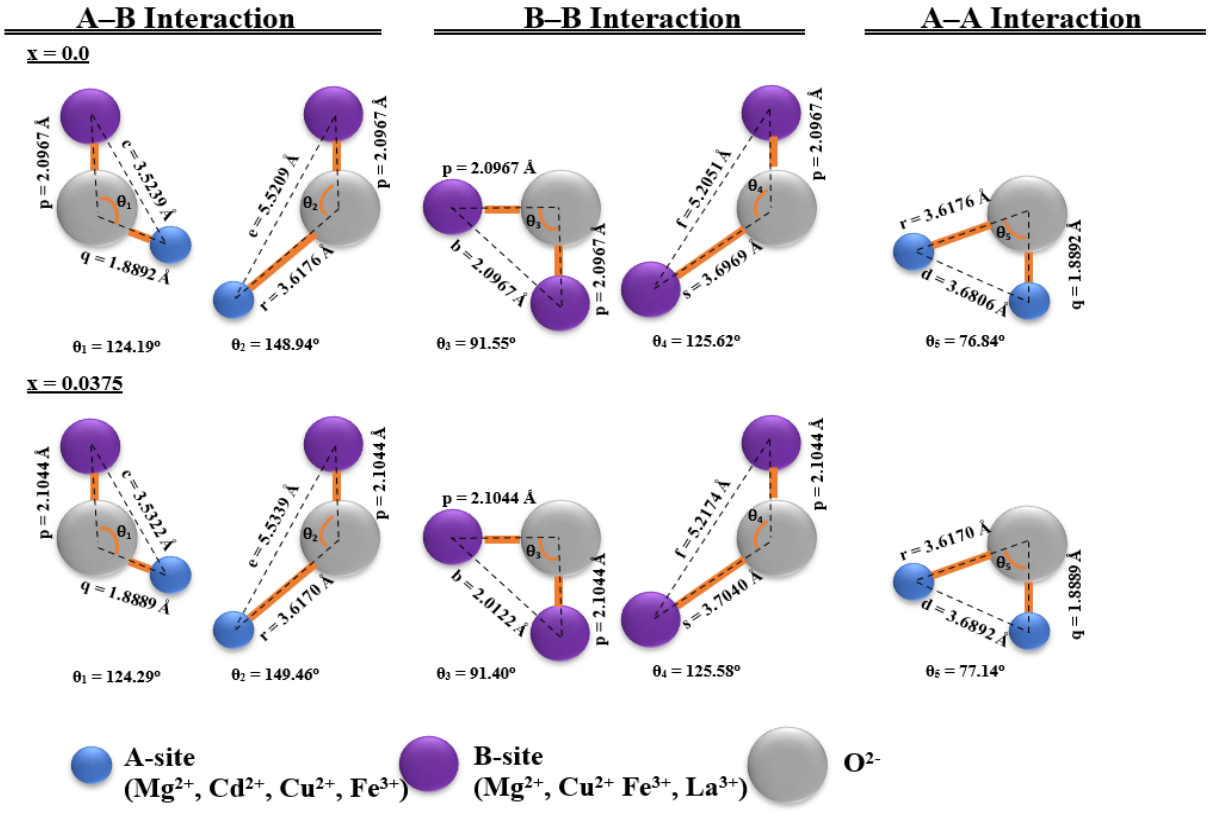


**Fig. 5** Interionic distance and bond angles relation

## 3.2 FTIR Analysis

The absorption bands and functional group analysis of $La^{3+}$ doped Mg-Cd-Cu ferrites were studied by FTIR and the results are presented in Fig. 6. Two most prominent frequency bands

$\upsilon_2$ in between 415.01 – 470.90 $cm^{-1}$ related to the octahedral site having oxygen octahedron (O – Fe – O) vibrations and $\upsilon_1$ in between 528.06 – 538.08 $cm^{-1}$ being specified to the tetrahedral site having oxygen tetrahedron (Fe – O) vibrations [44] are seen confirming the $La^{3+}$ doping in spinel matrix and similar trend reported in the literature [38]. It can be seen from Table 9 that the frequency band range for both $\upsilon_2$ and $\upsilon_1$ increases with the addition of $La^{3+}$ contents. As $Mg^{2+}$ and $Cu^{2+}$ partially occupy tetrahedral sites, the insertion of $La^{3+}$ does bring remarkable deviations in the octahedral site and confirmed the substitution of $La^{3+}$ ions at the spinel lattice. Bands occurring at 3750 $cm^{-1}$ and 1500 $cm^{-1}$ are due to O –H stretching vibrations [45]. The values of the force constants at the tetrahedral site ($K_T$) increased from $2.5769\times10^2$ N/m to $2.6757\times10^2$ N/m and at the octahedral site ($K_o$) increased from $1.5917\times10^2$ N/m and $2.0492\times10^2$ N/m with the doping of $La^{3+}$ ions.

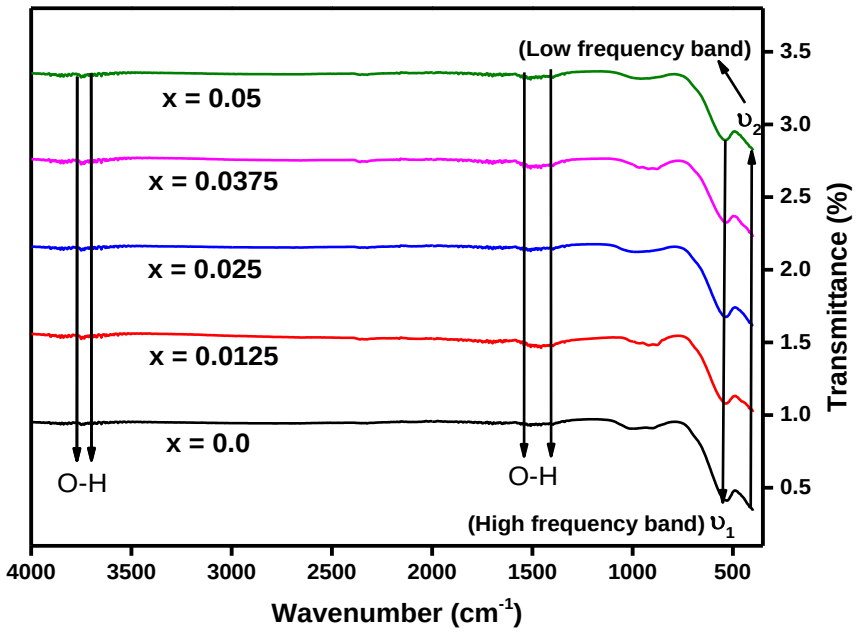


**Fig. 6** FTIR spectrum of $La^{3+}$ doped Mg-Cd-Cu ferrite samples

**Table 9** Absorption band positions, Force constants ($K_T$ and $K_o$) for as-prepared samples

| x | $\upsilon_1$ ($cm^{-1}$) | $K_T$ $\times10^2$ N/m | $\upsilon_2$ ($cm^{-1}$) | $K_o$ $\times10^2$ N/m |
|---|---|---|---|---|
| 0.00 | 528.06 | 2.5769 | 415.01 | 1.5917 |
| 0.0125 | 533.78 | 2.6331 | 428.98 | 1.7006 |
| 0.0250 | 535.22 | 2.6473 | 441.79 | 1.8037 |
| 0.0375 | 536.65 | 2.6615 | 455.47 | 1.9171 |
| 0.0500 | 538.08 | 2.6757 | 470.90 | 2.0492 |

### 3.3 Lattice structure and Molecular Vibration analysis

To have information on the lattice structure and vibrational possession properties of the $La^{3+}$ substituted in Mg-Cd-Cu soft ferrite samples, the Raman scattering experiments were carried out and the Lorentz fit spectra [46-48] of the ferrites in the range of 250-800 $cm^{-1}$, is represented in Fig. 7. The crystal structure of the inverse cubic spinel ferrites is a part of the (*F d -3 m*) space group having eight formula units per unit cell. The complete unit cell of cubic symmetric consists of 56 atoms, but the Bravais cell of a small scale consists of 14 atoms. So, there are almost 42 vibrational modes. Group theory anticipated the subsequent optical phonon distribution: $A_{1g}(R) + E_g(R) + T_{1g} + 3T_{2g}(R) + 2A_{2u} + 2E_u + 5T_{1u}(IR) + 2T_{2u}$ [47].

The mutual exclusion of Raman (R) and Infrared (IR) activities is shown by the presence of an inversion center in the centro-symmetrical space group *F d* -3 *m* for the same vibrational mode. The five first active modes in the Raman spectrum at 303 K are $A_{1g}$ (R), $E_g$ (R), and $3T_{2g}$ (R). The notations A, E, and T denote one, two, and three-dimensional representations, respectively, as well as "g", which represents symmetry to the center of inversion [49, 50]. The interpretation founded on the quasi-molecular characterization of spinel structure correlated to the normal mode motions of the tetrahedron ($Fe\text{-}O_4$) in the following way: The $A_{1g}$ (1) is due to symmetric stretching of oxygen atoms ahead Fe-O tetrahedral bonds and occurred at 665.53-684.70 $cm^{-1}$ with respect to the metal ion in tetrahedral (A) site [51, 52], $E_g$ and $T_{2g}$ (3) are assigned to symmetric and asymmetric bending of oxygen at the octahedral (B) site [51, 52] relative to Fe appeared at 328.60-398.11 $cm^{-1}$ and 533.85-544.28 $cm^{-1}$, respectively. $T_{2g}$ (2) is assigned to asymmetric stretching of Fe-O bond also at the octahedral (B) site [51, 52] and found at 459.65-471.51 $cm^{-1}$, and $T_{2g}$ (1) is assigned to translational motion of complete tetrahedron [51, 52] ($Fe\text{-}O_4$) and present at 292.10-319.99 $cm^{-1}$. The observed values are reported in Table 10. In the Raman spectra of $La^{3+}$ doped Mg-Cd-Cu ferrite samples, the five Raman active modes can be observed together with some extra vibrational bands other than the active ones. Here, the presence of these modes is generally assigned to the dislocations or impurities present in the matrix. The Raman active modes appeared because of the polarizability change in the course of molecular vibration in the structure, which was based on a loss of symmetry, activating the Raman modes [50, 53]. The doping in spinel ferrites does not affect the number of modes but results in a shift in their values. This factor is based on the position of ions in the crystal lattice and apparent mass in the crystal field. The intensive Raman peaks are attributed to the asymmetric reaction of the structure via vibrating dipole. Hence the expansion gives rise to the idea of a deformed matrix.

The doping of copper didn't alter the space group of spinel structure but deformed the crystal matrix of vibrating molecules. The vibrational modes that occurred above 600 $cm^{-1}$ are attributed to the translatory movement of the A-site that is engaged by oxygen in the $AO_4$ composites [54, 55].

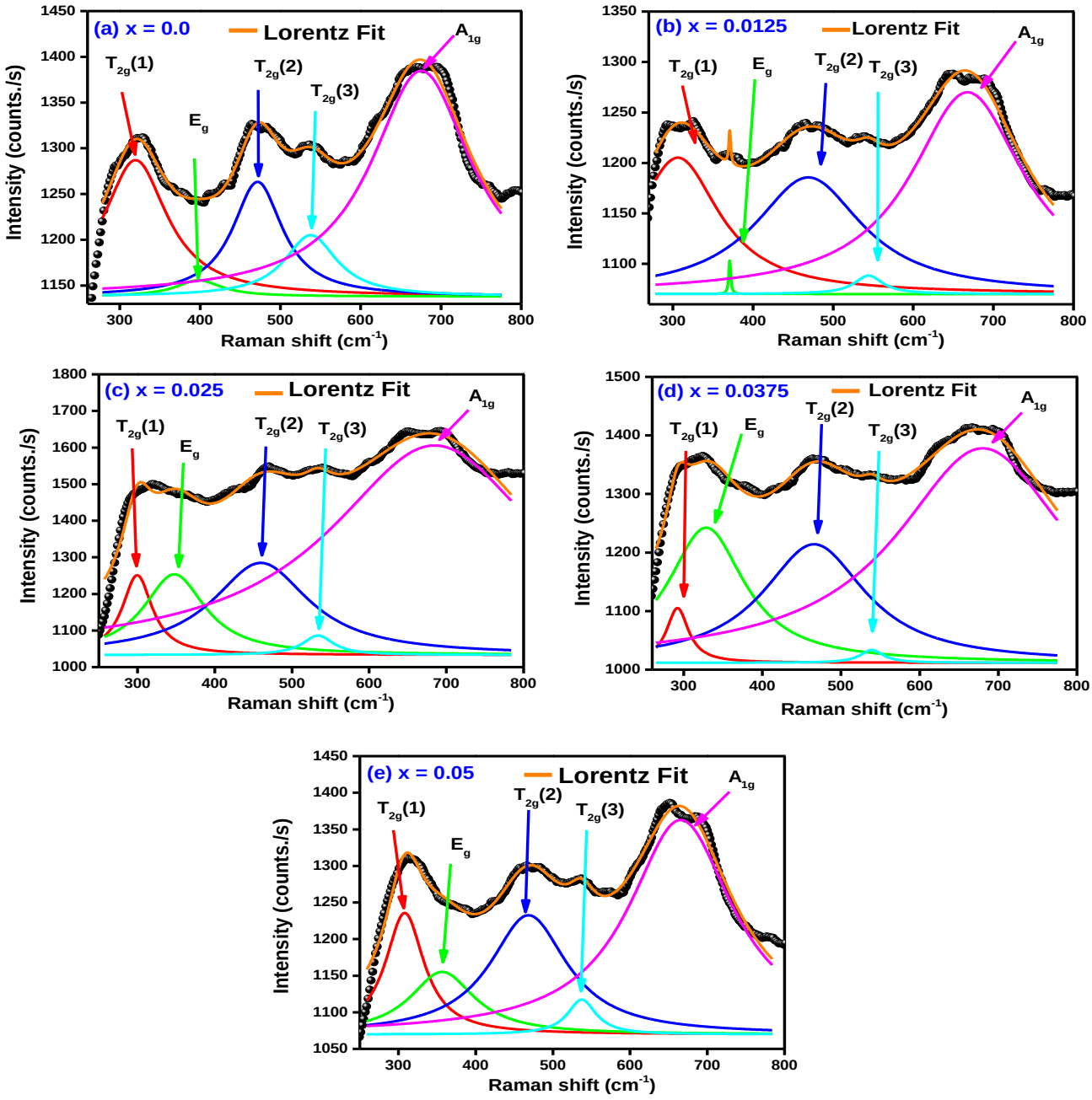


**Fig. 7** Raman spectra for $La^{3+}$ doped Mg-Cd-Cu ferrite samples

**Table 10** Raman modes for $La^{3+}$ doped Mg-Cd-Cu ferrite samples

| x | Raman shift ($cm^{-1}$) | | | | |
|---|---|---|---|---|---|
| | $T_{2g}$ (1) | $E_g$ | $T_{2g}$ (2) | $T_{2g}$ (3) | $A_{1g}$ |
| | Tetrahedral (A) Site [51, 52] | | octahedral (B) site [51, 52] | | Tetrahedral (A) Site [51, 52] |
| 0.0 | 319.99 | 398.11 | 471.51 | 537.69 | 675.46 |
| 0.0125 | 306.29 | 371.03 | 469.08 | 544.28 | 667.73 |
| 0.025 | 299.62 | 347.70 | 459.65 | 533.85 | 684.70 |
| 0.0375 | 292.10 | 328.60 | 465.82 | 539.22 | 680.16 |
| 0.05 | 308.14 | 356.63 | 468.45 | 537.42 | 665.53 |

## 3.4 Optical Study

The absorption coefficient (α) for $La^{3+}$ doped Mg-Cd-Cu ferrites was determined by employing the following equation [32]:

$$\alpha = 2.303 \frac{\log(A)}{l} \quad (1)$$

where 'A' indicates absorbance and '$l$' is the path length of light in which absorbance takes place. To find optical bandgap energy ($E_g$), Tauc's relation narrated to photon energy and absorbance was employed as [32]:

$$E_g = \frac{hv}{\lambda} \quad (2)$$

$$\alpha hv = B(hv - Eg)^m \quad (3)$$

where 'B' is the transition probability dependence constant, 'h' is the Planck constant, '$v$' is the frequency, and 'm' is the number that expresses the absorption transition process.

From the using equation 4.3, the Tauc-plots are represented in Fig. 8 from which the optical band gap ($E_g$) is determined being 3.03 eV, 3.29 eV, 2.95 eV, 3.38 eV, 3.18 eV, with the substitution of $La^{3+}$ ions. It can be seen that the optical band gap reduced up to x = 0.025 and then increased with the addition of $La^{3+}$ contents. Such an increase in the bandgap would potentially make the material being applicable in microwave frequency devices [56]. Another optical band gap ($E_g'$) is also emerging inside of the plots for x = 0.0 – 0.05 as expressed in Fig. 8 and their values with increasing x are 2.50 eV, 2.37 eV, 2.17 eV, 1.95 eV, 2.20 eV. The optical band gap firstly decreases and then increases is maybe due to dopant ion concentration, lattice strain, lattice structural parameters, the presence of impurities, and surficial impact [57]. Here, the fact that $E_g'$ being lower than $E_g$ is associated with the impurity phases because of the charge transfers amongst $Fe^{3+}/La^{3+}$ at the octahedral site. At the tetrahedral site, the charge

exchange energy is not much influenced by the $La^{3+}$ insertion, while on the octahedral site, charge exchange energy is larger [58]. Furthermore, a hump appearing at the mid of the curves is increasing with the increase of $La^{3+}$ contents and similar behavior reported in the literature [57].

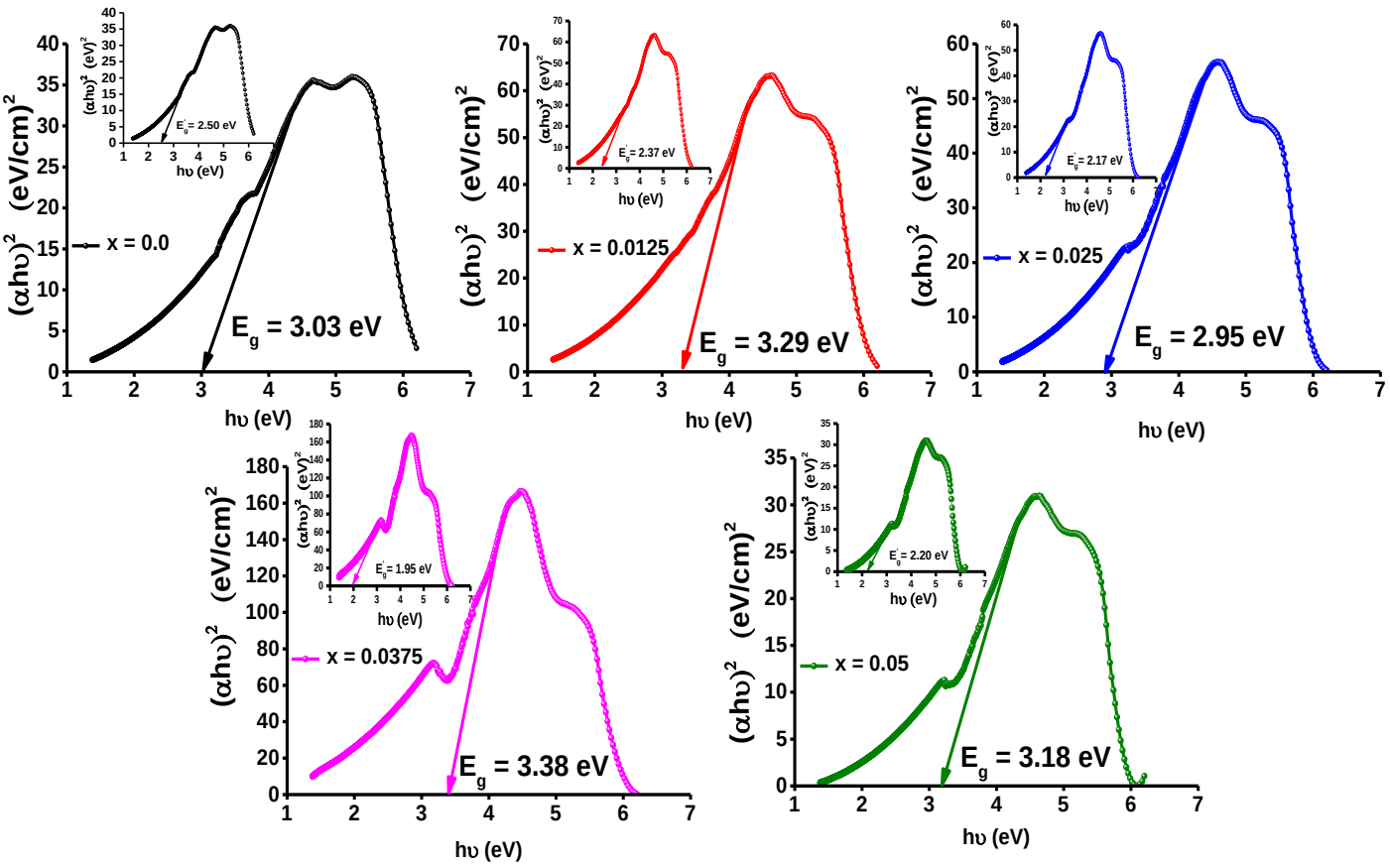


**Fig. 8** Tauc-plot for optical band gap (Eg and $E'_g$) of $La^{3+}$ doped Mg-Cd-Cu ferrite samples

## 3.5 Electrical Analysis

Two probes current-voltage (I-V) measurements were employed to study electrical properties of $La^{3+}$ doped Mg-Cd-Cu ferrites in the temperature range of 303–823 K and the results of DC electrical resistivity ($\rho_{DC}$) *versus* 1000/T are presented in Fig. 9. Here the Curie temperature was determined from the kink as shown in the ($\rho_{DC}$) *versus* 1000/T curves, and it can be seen that it rises with increasing La doping being 363 K, 383 K, 403 K, 423 K, and 453 K for x = 0.00, 0.0125, 0.025, 0.0375, 0.05, respectively. It can be seen that, in the ferromagnetic region, the resistivity increases with increasing temperature, whereas it becomes the opposite in the paramagnetic region, which is consistent with that reported in the literature

[59]. The decline in resistivities at high temperatures shows the semiconducting nature of the fabricated soft-ferrites. The observed reduction in resistivity at high temperatures could be due to the rise in drift mobility of thermally activated charge carriers, which depends on impurities, particle size, density, etc. [60]. The "$\rho_{DC}$" at RT for all the samples are 2.67 × $10^4$ Ω cm, 8.94 × $10^3$ Ω cm, 7.95 × $10^4$ Ω cm, 2.68 × $10^3$ Ω cm and 1.40 × $10^4$ Ω cm for x = 0.00, 0.0125, 0.025, 0.0375, 0.05, respectively. The maximum resistivity occurs for the sample with x = 0.025, and it would make the material more suitable for use in high-frequency electronic devices [61].

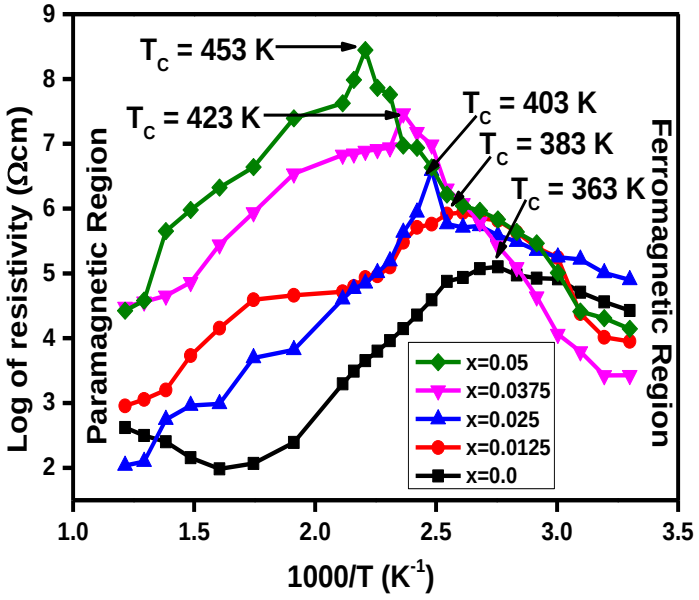


**Fig. 9** 1000/T *versus* the log of resistivity of $La^{3+}$ doped Mg-Cd-Cu soft ferrite samples

The results of the resistivity *versus* concentration of doped $La^{3+}$ at different temperatures in the ferromagnetic and paramagnetic regions are presented in Fig. 10. It can be seen that at x = 0.025, the resistivity has a maximum value in the ferromagnetic region and the minimum value in the paramagnetic region. The resistivity has lower values in paramagnetic region before x = 0.025 but then it becomes higher values for x = 0.0375 and 0.05 in the ferromagnetic region (Fig. 10a). In the ferromagnetic region (Fig. 10b), the resistivity has random behavior, but as the temperature increases up to 373 K, it becomes almost constant with respect to the $La^{3+}$ content. After $T_c$ = 373 K, the resistivities tend to increase with increasing $La^{3+}$ concentrations.

The Arrhenius equation ($\rho = \rho_0 e^{-\frac{\Delta E}{k_B T}}$) was employed to investigate the activation energies for all $La^{3+}$ concentrations. The activation energies in the paramagnetic region ($E_p$) are seen greater than those in the ferromagnetic region ($E_f$) in accordance with the Irkhin and Turov theory and affirms the ordering and disordering arrangements of atoms in paramagnetic

and ferromagnetic states, respectively [62, 63]. In a paramagnetic state, charge carriers required more energy to transfer than those in the ferromagnetic state where the conduction procedures in soft ferrites are manipulated through the magnetic arrangements [64]. The activation energy ($\Delta E=E_p-E_f$) *versus* $La^{3+}$ doped concentration is presented in Fig. 11. In the ferrites, the conductivity depends on activation energy, and the nonlinearity in $\Delta E$ with the insertion of $La^{3+}$ might be related to the effect of spin disordering [65-67]. The high resistivity ranges observed in our synthesized ferrites make them potentially applicable in telecommunication devices [66, 67].

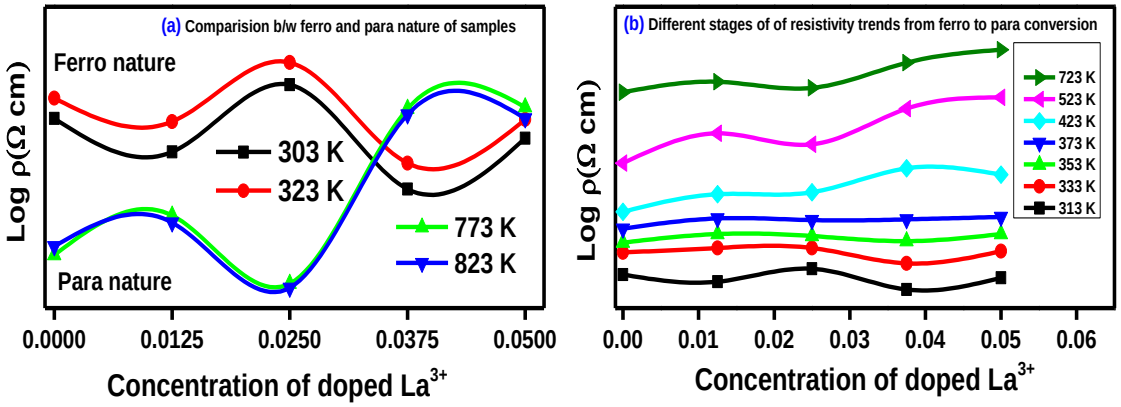


**Fig. 10** Log of resistivity *versus* $La^{3+}$ concentration at various temperatures of $La^{3+}$ doped Mg-Cd-Cu soft ferrite samples: **a)** comparison between ferromagnetic and paramagnetic nature, **b)** $La^{3+}$ concentration *versus* resistivity at different temperatures

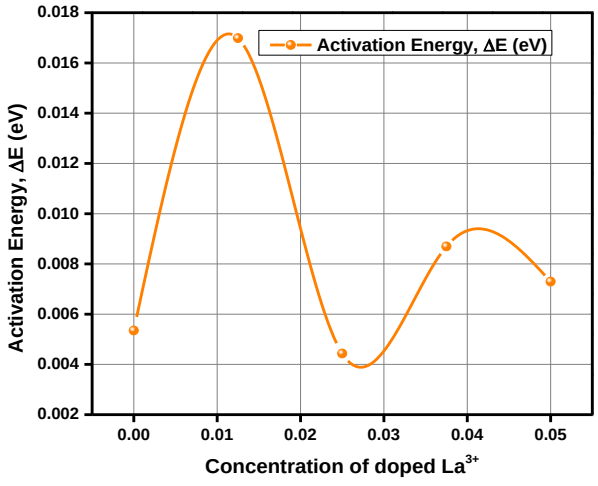


**Fig. 11** Activation energy $\Delta E$ *versus* $La^{3+}$ doped concentration in Mg-Cd-Cu soft ferrite samples

The drift mobility ($\mu_d$) for all the samples have values $3.84 \times 10^{-18}$ $cm^2V^{-1}s^{-1}$ (x = 0), $11.5 \times 10^{-18}$ $cm^2V^{-1}s^{-1}$(x = 0.0125), $1.31\times 10^{-18}$ $cm^2V^{-1}s^{-1}$ (x = 0.025), $38.9 \times 10^{-18}$ $cm^2V^{-1}s^{-1}$ (x =

0.0375) and 7.52 × $10^{-18}$ $cm^2V^{-1}s^{-1}$ (x = 0.05). It is clear that the samples with greater electrical resistivity have small value of drift mobility, and *vice versa*, because both drift mobility and electrical resistivity have inverse relation [68, 69].

## 3.6 Dielectric Analysis

In the ferrites, dielectric properties are influenced by the fabrication mechanism, sintering temperature, nature of materials, and compositional variations [70]. The dielectric tangent loss (tan δ) as a function of applied frequency is shown in Fig. 12. The polarization occurred because of the intra-grain conduction by exchange interaction, which is responsible for the dielectric loss tangent. A barrier is formed at the grain boundary because of the space charge of the accumulated electrons, which restricts the inside grain conduction of soft ferrites. Therefore, a large number of electrons accumulated, and more will be the space charges at the grain boundary. When the grain boundary conduction occurred, the polarization decreased and resulted in the dominance of inside grain conductions due to a small barrier; hence, the strength of the barrier will be reduced. This decreased grain boundary polarizability appears as the tan δ loss [71]. It can be seen from Fig. 12 that due to space charge polarization, the dielectric loss tangent rapidly decreases for low frequency and the rate of reduction in tan δ is slow at high frequency. Minimal values are observed in the frequency range from 6 to 7 MHz, which are ideal for high-frequency applications [72].

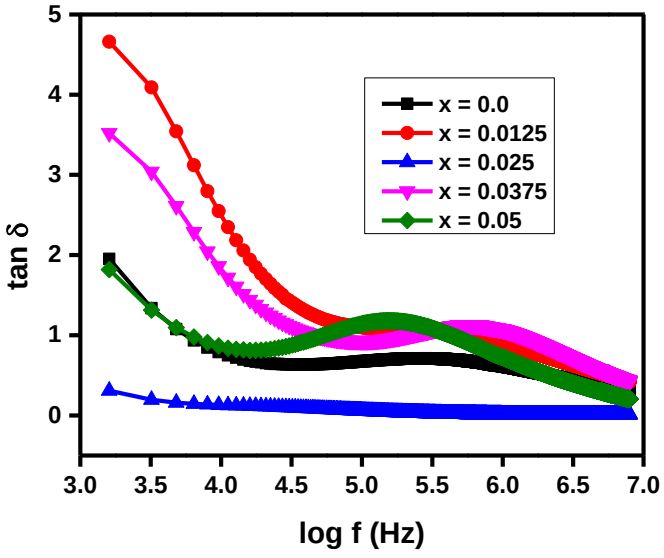


**Fig. 12**. The dependence of dielectric tangent loss *versus* applied frequency $La^{3+}$ doped Mg-Cd-Cu soft ferrite samples

The concentration of doped $La^{3+}$ *versus* dielectric tangent loss at different applied frequencies is depicted in Fig. 13(a-c). It can be seen in Fig. 13(a-c) that the "tanδ" has a

minimum for $La^{3+}$ concentration x = 0.025. On the other hand, at low frequency (Fig. 13(a)) the maximum dielectric tangent loss was observed for $La^{3+}$ concentration x = 0.0125 and at a medium range of frequency (Fig. 13(b)), the "tan δ" has maximum value for $La^{3+}$ concentration x = 0.05. It was observed from Fig. 13(c) at high frequency the "tan δ" has a large value for $La^{3+}$ concentration x = 0.0375.

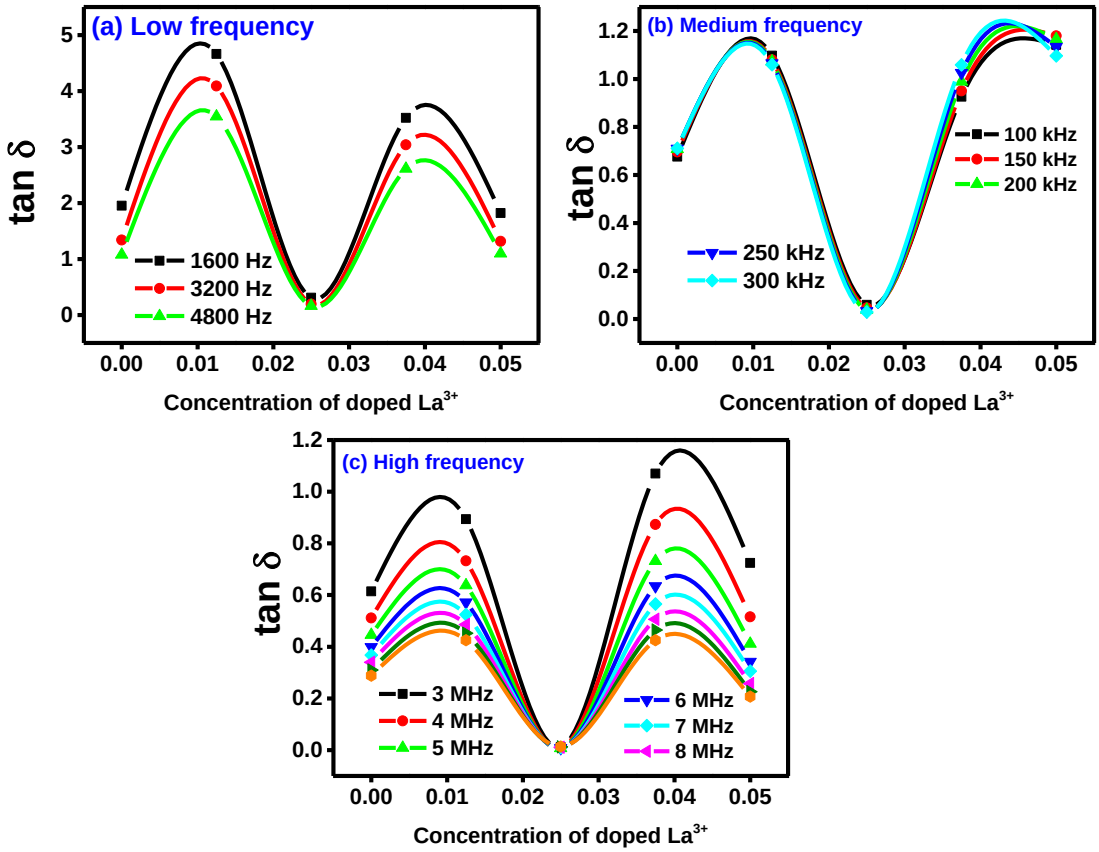


**Fig. 13(a-c)** Concentration of doped $La^{3+}$ *versus* dielectric tangent loss at the different applied frequency

## 3.7 Magnetic Properties

The magnetic hysteresis loops of $La^{3+}$ doped Mg-Cd-Cu ferrites measured at RT are presented in Fig. 14. From the hysteresis loops, the values of coercivity ($H_c$), remnant squareness (SQ or $M_r/M_s$) remanent magnetization ($M_r$), and saturation magnetization ($M_S$) are obtained and reported in Table 11. In Mg–Cd–Cu ferrites, the $Mg^{2+,}$ and $Fe^{3+}$ ions share A and B sites in the spinel structure. The insertion of paramagnetic $La^{3+}$ ions enhance $M_s$ from 15.4057 (x = 0) to 49.3850 emu/g (x = 0.05). On the other hand, the coercivity is seen to decrease with increasing $La^{3+}$ content from 793.1 Oe (x = 0) to 661.4 Oe (x = 0.05). The change

in coercivity is due to the combination of different factors, including particle size, crystallinity, crystal structure, morphology, strain, and anisotropy [56]. For the squareness ratio (SQ or $M_r/M_s$), the obtained values are in the range of 0.6505-0.7869. The small value of the SQ ratio shows that the as-prepared samples are single domains [22]. The trends of coercivity, saturation magnetization, and remanence indicate that higher spin-orbital coupling is created by $La^{3+}$ ions at the octahedral site as compared to bulk material [31, 73]. Magneto crystalline anisotropy constant (K) calculated using $K = \frac{H_c \times M_s}{0.96}$ and initial permeability ($\mu_i$) calculated via $\mu_i = \frac{M_s^2 \times D}{K}$ are also given in Table 11. It was observed that the anisotropy constant K as well as $\mu_i$ increase with increasing $La^{3+}$ concentration. The Bohr's magneton ($n_B$) was calculated using $n_B = (M \times M_S)/(5585 d_x)$, where M, and $d_x$ are molecular weight, and X-ray density, respectively. It was found that Bohr's magneton increased from 0.1275 (x = 0) to 0.4156 (x = 0.05) which is because the doping of $La^{3+}$ results in a strong La–Fe interaction on the B site [30]. The spin canting angle known as Yafet and Kittel (Y–K) angles were determined using Yafet and Kittel model from $n_B = (6 + x)\cos\alpha_{y-k} - 5(1 - x)$. The calculated values of Y–K angles are also added in Table 11, which increases with $La^{3+}$ concentration indicating an increasing triangular spin arrangement at B-site in soft-ferrites. This improved triangular spin arrangement at B sites is responsible for decreasing A–B interaction in soft-ferrites [71]. The rare earth $La^{3+}$ ions have zero magnetic moments, and hence, A–B interaction become decreases as the concentration of $La^{3+}$ increased in Mg–Cd–Cu soft-ferrites. Microwave frequency can be studied through the application of the following relation $\omega_m = 8\pi^2 M_s \gamma$, where $\gamma$ is a gyromagnetic fraction with the significance of 2.8 MHz/Oe [23, 27, 31, 57]. The applied field *versus* microwaves operating frequency $\omega_m$ of $La^{3+}$ doped Mg-Cd-Cu ferrite samples is plotted in Fig. 15. With x from 0 to 0.05, $\omega_m$ can be found in the range of 3.36 – 10.80 GHz, indicating that $La^{3+}$ doped Mg-Cd-Cu ferrites are exceptionally applicable in longitudinal recording media and microwave absorbance purposes and similar behavior was reported in the literature for microwave applications [57].

**Table 11** Magnetic parameters for $La^{3+}$ doped Mg-Cd-Cu ferrite samples

| x | $H_C$ (Oe) | SQ | $M_r$ (emu/g) | $M_s$ (emu/g) | $n_B$ | K (erg/cm$^3$) | $\mu_i$ | $\alpha_{y-k}$ (Degree) | $\omega_m$ (GHz) |
|---|---|---|---|---|---|---|---|---|---|
| 0.00 | 793.1 | 0.6859 | 10.5669 | 15.4057 | 0.1275 | 12727.35 | 0.4936 | 31.2849 | 3.36 |
| 0.0125 | 780.5 | 0.6505 | 12.9106 | 19.8469 | 0.1642 | 16135.94 | 0.7173 | 31.9482 | 4.50 |
| 0.025 | 768.0 | 0.7055 | 15.7455 | 22.3167 | 0.1851 | 17853.36 | 0.9006 | 32.8743 | 4.89 |
| 0.0375 | 742.9 | 0.7869 | 28.4709 | 36.1794 | 0.3021 | 27997.57 | 1.1840 | 32.0969 | 7.99 |
| 0.05 | 661.4 | 0.7072 | 34.9283 | 49.3850 | 0.4156 | 34024.20 | 1.8637 | 31.3694 | 10.80 |

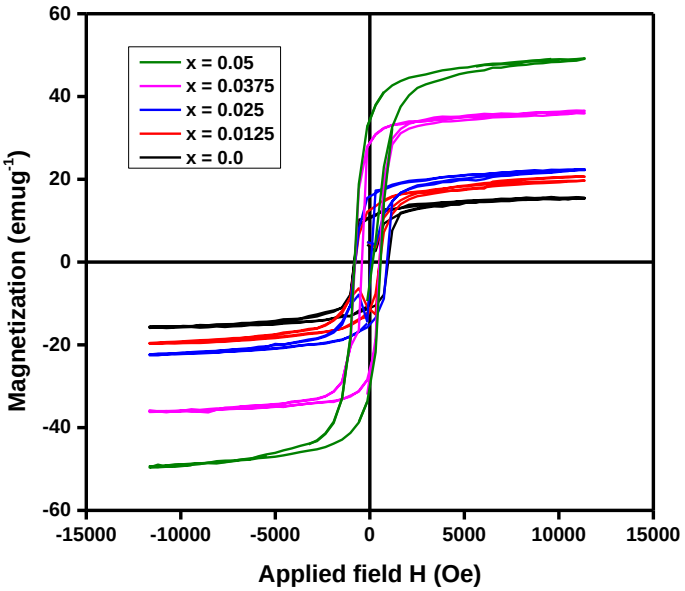


**Fig. 14** Hysteresis loops for $La^{3+}$ doped Mg-Cd-Cu ferrite samples

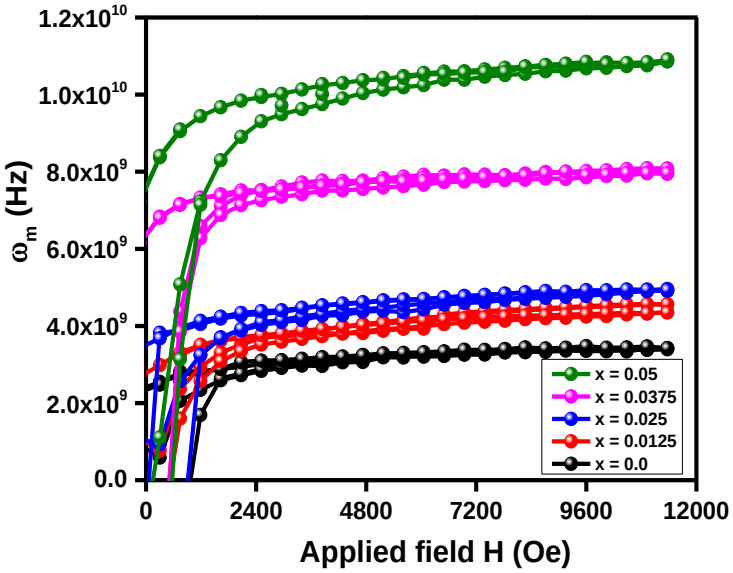


**Fig. 15** Applied field *versus* microwaves operating frequency of $La^{3+}$ doped Mg-Cd-Cu ferrite samples

### 3.8 Inductively Coupled Plasma Mass Spectroscopy (ICP-MS) Analysis

Inductively coupled plasma mass spectrometry was used to evaluate the chemical compositions (ICP-MS). In 1 mL of $HNO_3$, 2 mg of each powder sample was dissolved. Table 12 shows the findings of a study of the Fe, Mg, Cd, Cu, and La compositions of synthesized $La^{3+}$ doped Mg-Cd-Cu ferrite samples. The predicted value is based on the stoichiometry of

$La^{3+}$ doped Mg-Cd-Cu ferrites. It was observed that the stoichiometry is quite close to the expected values.

**Table 12** ICP measurements for $La^{3+}$ doped Mg-Cd-Cu ferrite samples

| x | Fe (µg per mL) | Cu (µg per mL) | Mg (µg per mL) | Cd (µg per mL) | La (µg per mL) |
|---|---|---|---|---|---|
| 0.0 | 1232.5 | 185.8 | 138.3 | 291.9 | 0.5 |
| 0.0125 | 1027.2 | 157.4 | 117.0 | 245.2 | 15.7 |
| 0.025 | 993.8 | 152.3 | 112.1 | 248.6 | 47.2 |
| 0.0375 | 893.5 | 137.0 | 103.5 | 419.9 | 38.6 |
| 0.05 | 945.5 | 142.4 | 107.9 | 432.4 | 61.0 |

## 4 Conclusions

$La^{3+}$ doped Mg-Cd-Cu ferrites were fabricated *via* co-precipitation. The structural parameters are dependent on $La^{3+}$ concentration. The existence of tetrahedral and octahedral bands was seen in the FTIR spectra. Considerable magnification in optical bandgap energy in the range of 2.95 – 3.38 eV was recorded due to the less conductive $La^{3+}$ ions doping. Electrical resistivity demonstrated the opposite trend in paramagnetic and ferromagnetic regions. Dielectric losses were revealed in declining order, with increasing frequency. The magnetic performances of $La^{3+}$ substituted Mg-Cd-Cu ferrites are enhanced with an increase in saturation ($M_s$) and remanence ($M_r$) magnetization. The calculated frequency range of $La^{3+}$ inserted spinel ferrites by the application of $M_s$ was detected in the microwave range of 3.36 – 10.80 GHz. From the results of our studies, the $La^{3+}$ doped spinel ferrites appear to be highly applicable in longitudinal recording media and microwave absorbance.

## Acknowledgement

NT KT thanks EPSRC, UK (EP/M015157/1), NTKT, and LDT would like to thank AOARD (FA2386-17-1-4042 award) for financial support.

## References

[1] M. Rashad, D. Rayan, A. Turky, M. Hessien, Effect of $Co^{2+}$ and $Y^{3+}$ ions insertion on the microstructure development and magnetic properties of $Ni_{0.5}Zn_{0.5}Fe_2O_4$ powders synthesized using co-precipitation method, Journal of Magnetism and Magnetic Materials, 374 (2015) 359-366.

[2] M. Ahmed, H. Hassan, M. Eltabey, K. Latka, T. Tatarchuk, Mössbauer spectroscopy of $Mg_xCu_{0.5-x}Zn_{0.5}Fe_2O_4$ (x = 0.0, 0.2 and 0.5) ferrites system irradiated by γ-rays, Physica B: Condensed Matter, 530 (2018) 195-200.

[3] W. Hu, N. Qin, G. Wu, Y. Lin, S. Li, D. Bao, Opportunity of spinel ferrite materials in nonvolatile memory device applications based on their resistive switching performances, Journal of the American Chemical Society, 134 (2012) 14658-14661.

[4] S. Kane, M. Satalkar, Correlation between magnetic properties and cationic distribution of $Zn_{0.85-x}Ni_xMg_{0.05}Cu_{0.1}Fe_2O_4$ nano spinel ferrite: effect of Ni doping, Journal of materials science, 52 (2017) 3467-3477.

[5] S. Patil, H.B. Naik, G. Nagaraju, R. Viswanath, S. Rashmi, Synthesis of visible light active $Gd^{3+}$-substituted $ZnFe_2O_4$ nanoparticles for photocatalytic and antibacterial activities, The European Physical Journal Plus, 132 (2017) 328.

[6] R. Sharma, P. Thakur, M. Kumar, P. Sharma, V. Sharma, Nanomaterials for high frequency device and photocatalytic applications: Mg-Zn-Ni ferrites, Journal of Alloys and Compounds, 746 (2018) 532-539.

[7] S.F. Wang, Y.J. Chiang, Y.F. Hsu, C.H. Chen, Effects of additives on the loss characteristics of Mn–Zn ferrite, Journal of Magnetism and Magnetic Materials, 365 (2014) 119-125.
[8] P. Hankare, U. Sankpal, R. Patil, I. Mulla, P. Lokhande, N. Gajbhiye, Synthesis and characterization of $CoCr_xFe_{2-x}O_4$ nanoparticles, Journal of Alloys and Compounds, 485 (2009) 798-801.
[9] S. Giri, S. Samanta, S. Maji, S. Ganguli, A. Bhaumik, Magnetic properties of α-$Fe_2O_3$ nanoparticle synthesized by a new hydrothermal method, Journal of Magnetism and Magnetic Materials, 285 (2005) 296-302.
[10] P. Singjai, K. Wongwigkarn, Y. Laosiritaworn, R. Yimnirun, S. Maensiri, Carbon encapsulated nickel nanoparticles synthesized by a modified alcohol catalytic chemical vapor deposition method, Current Applied Physics, 7 (2007) 662-666.
[11] R. Zakir, S.S. Iqbal, A.U. Rehman, S. Nosheen, T.S. Ahmad, N. Ehsan, F. Inam, Spectral, electrical, and dielectric characterization of Ce-doped Co-Mg-Cd spinel nano-ferrites synthesized by the sol-gel auto combustion method, Ceramics International, 47 (2021) 28575-28583.
[12] M. George, A.M. John, S.S. Nair, P. Joy, M. Anantharaman, Finite size effects on the structural and magnetic properties of sol–gel synthesized $NiFe_2O_4$ powders, Journal of Magnetism and Magnetic Materials, 302 (2006) 190-195.
[13] R. Krishnakanth, G. Jayakumar, A.A. Irudayaraj, A.D. Raj, Structural and magnetic properties of NiO and Fe-doped NiO nanoparticles synthesized by chemical co-precipitation method, Materials Today: Proceedings, 3 (2016) 1370-1377.
[14] T.M. Hammad, J.K. Salem, A.A. Amsha, N.K. Hejazy, Optical and magnetic characterizations of zinc substituted copper ferrite synthesized by a co-precipitation chemical method, Journal of Alloys and Compounds, 741 (2018) 123-130.
[15] N. Amin, M. Akhtar, M. Sabir, K. Mahmood, A. ALIa, G. Mustafa, M. Hasan, A. Bibi, M. F. Iqbal, SYNTHESIS, STRUCTURAL AND OPTICAL PROPERTIES OF Zn-SUBSTITUTED Co W-FERRITES BY COPRECIPITATION METHOD, Journal of Ovonic Research, 16 (2020) 11-19.
[16] I. ALIa, N. Amin, A. REHMAN, M. Akhtar, M. Fatima, K. Mahmood, A. ALIa, G. Mustafa, M. Hasan, A. Bibi, Biostructures, ELECTRICAL AND MAGNETIC PROPERTIES OF $BaCo_xCd_{2-x}Fe_{16}O_{27}$ W-TYPE HEXAFERRITES ($0 \leq x \leq 0.5$), Digest Journal of Nanomaterials & Biostructures, 15 (2020).
[17] N. Amin, M.S.U. Hasan, Z. Majeed, Z. Latif, M.A. un Nabi, K. Mahmood, A. Ali, K. Mehmood, M. Fatima, M. Akhtar, Structural, electrical, optical and dielectric properties of yttrium substituted cadmium ferrites prepared by Co-Precipitation method, Ceramics International, 46(13), (2020) 20798-20809.
[18] H.T. Ali, M. Ramzan, M.I. Arshad, N.A. Morley, M.H. Abbas, M. Yusuf, A.U. Rehman, K. Mahmood, A. Ali, N. Amin, Tailoring the optical, and magnetic properties of La-BaM hexaferrites by Ni substitution, Chinese Physics B, (2021). https://doi.org/10.1088/1674-1056/ac1412
[19] M. Hasan, M. Arshad, A. Ali, K. Mahmood, N. Amin, S. Ali, M. Khan, G. Mustafa, M. Khan, M. Saleem, Mg and La co-doped ZnNi spinel ferrites for low resistive applications, Materials Research Express, 6 (2018) 016302.
[20] Y. Kannan, R. Saravanan, N. Srinivasan, K. Praveena, K. Sadhana, Synthesis and characterization of some ferrite nanoparticles prepared by co-precipitation method, Journal of Materials Science: Materials in Electronics, 27 (2016) 12000-12008.
[21] R.R. Kanna, K. Sakthipandi, S.S.M.A. Maraikkayar, N. Lenin, M. Sivabharathy, Doping effect of rare-earth (lanthanum, neodymium and gadolinium) ions on structural, optical, dielectric and magnetic properties of copper nanoferrites, Journal of Rare Earths, 36 (2018) 1299-1309.
[22] S. Ikram, M.I. Arshad, K. Mahmood, A. Ali, N. Amin, N. Ali, Structural, magnetic and dielectric study of $La^{3+}$ substituted $Cu_{0.8}Cd_{0.2}Fe_2O_4$ ferrite nanoparticles synthesized by the co-precipitation method, Journal of Alloys and Compounds, 769 (2018) 1019-1025.
[23] S. Gaba, A. Kumar, P.S. Rana, M. Arora, Influence of $La^{3+}$ ion doping on physical properties of magnesium nanoferrites for microwave absorption application, Journal of Magnetism and Magnetic Materials, 460 (2018) 69-77.
[24] B. Patil, A. Pawar, D. Bhosale, J. Ghodake, J. Thorat, T. Shinde, Effect of $La^{3+}$ substitution on structural and magnetic parameters of Ni–Cu–Zn nano-ferrites, Journal of Nanostructure in Chemistry, 9 (2019) 119-128.
[25] V. Chaudhari, S.E. Shirsath, M. Mane, R. Kadam, S. Shelke, D. Mane, Crystallographic, magnetic and electrical properties of $Ni_{0.5}Cu_{0.25}Zn_{0.25}La_xFe_{2-x}O_4$ nanoparticles fabricated by sol–gel method, Journal of Alloys and Compounds, 549 (2013) 213-220.
[26] X. Zhou, J. Jiang, L. Li, F. Xu, Preparation and magnetic properties of La-substituted Zn–Cu–Cr ferrites via a rheological phase reaction method, Journal of magnetism and magnetic materials, 314 (2007) 7-10.
[27] A.U. Rehman, N. Amin, M.B. Tahir, M.A. un Nabi, N. Morley, M. Alzaid, M. Amami, M. Akhtar, M.I. Arshad, Evaluation of spectral, optoelectrical, dielectric, magnetic, and morphological properties of $RE^{3+}$ ($La^{3+}$, and $Ce^{3+}$) and $Co^{2+}$ co-doped $Zn_{0.75}Cu_{0.25}Fe_2O_4$ ferrites, Materials Chemistry and Physics, (2021) 125301.

[28] A. Aslam, N. Morley, N. Amin, M.I. Arshad, M.A. un Nabi, A. Ali, K. Mahmood, A. Bibi, F. Iqbal, S. Hussain, Study of structural, optical and electrical properties of $La^{3+}$ doped $Mg_{0.25}$ $Ni_{0.15}Cu_{0.25}Co_{0.35}Fe_{2-x}La_xO_4$ spinel ferrites, Physica B: Condensed Matter, 602 (2021) 412565.
[29] A.U. Rehman, N. Morley, N. Amin, M.I. Arshad, M.A. un Nabi, K. Mahmood, A. Ali, A. Aslam, A. Bibi, M.Z. Iqbal, Controllable synthesis of $La^{3+}$ doped $Zn_{0.5}Co_{0.25}Cu_{0.25}Fe_{2-x}La_xO_4$ (x = 0.0, 0.0125, 0.025, 0.0375, 0.05) nano-ferrites by sol-gel auto-combustion route, Ceramics International, 46 (2020) 29297-29308.
[30] A. Gadkari, T. Shinde, P. Vasambekar, Synthesis, characterization and magnetic properties of $La^{3+}$ added Mg–Cd ferrites prepared by oxalate co-precipitation method, Journal of alloys and compounds, 509 (2011) 966-972.
[31] A. Majeed, M.A. Khan, F. ur Raheem, A. Hussain, F. Iqbal, G. Murtaza, M.N. Akhtar, I. Shakir, M.F. Warsi, Structural elucidation and magnetic behavior evaluation of rare earth (La, Nd, Gd, Tb, Dy) doped BaCoNi-X hexagonal nano-sized ferrites, Journal of Magnetism and Magnetic Materials, 408 (2016) 147-151.
[32] A. Aslam, A.U. Rehman, N. Amin, M. Amami, M. Nabi, H. Alrobei, M. Asghar, N. Morley, M. Akhtar, M.I. Arshad, Sol–Gel Auto-combustion Preparation of $M^{2+}$= $Mg^{2+}$, $Mn^{2+}$, $Cd^{2+}$ Substituted $M_{0.25}Ni_{0.15}Cu_{0.25}Co_{0.35}Fe_2O_4$ Ferrites and Their Characterizations, Journal of Superconductivity and Novel Magnetism, (2021) 1-11.
[33] P. Puspitasari, U.A. Rizkia, S. Sukarni, A.A. Permanasari, A. Taufiq, A.B.N.R. Putra, Effects of Various Sintering Conditions on the Structural and Magnetic Properties of Zinc Ferrite ($ZnFe_2O_4$), Materials Research, 24 (2021).
[34] A. Aslam, A. Razzaq, S. Naz, N. Amin, M.I. Arshad, M.A.U. Nabi, A. Nawaz, K. Mahmood, A. Bibi, F. Iqbal, Impact of Lanthanum-Doping on the Physical and Electrical Properties of Cobalt Ferrites, Journal of Superconductivity and Novel Magnetism, (2021), 1-10.
[35] K. Hussain, N. Amin, M.I. Arshad, Evaluation of structural, optical, dielectric, electrical, and magnetic properties of $Ce^{3+}$ doped $Cu_{0.5}Cd_{0.25}Co_{0.25}Fe_{2-x}O_4$ spinel nano-ferrites, Ceramics International, 47 (2021) 3401-3410.
[36] N. Amin, A. Razaq, A.U. Rehman, K. Hussain, M. Nabi, N. Morley, M. Amami, A. Bibi, M.I. Arshad, K. Mahmood, Transport Properties of Ce-Doped Cd Ferrites $CdFe_{2-x}Ce_xO_4$, Journal of Superconductivity and Novel Magnetism, (2021) 1-11.
[37] M. Tufiq Jamil, J. Ahmad, S. Hamad Bukhari, M. Saleem, Effect of Re and Tm-site on morphology structure and optical band gap of $ReTmO_3$ (Re = La, Ce Nd, Gd, Dy, Y and Tm= Fe, Cr) prepared by sol-gel method, Revista mexicana de física, 64 (2018) 381-391.
[38] A. Aslam, A.U. Rehman, N. Amin, M.A. un Nabi, Q. ul ain Abdullah, N. Morley, M.I. Arshad, H.T. Ali, M. Yusuf, Z. Latif, Lanthanum doped $Zn_{0.5}Co_{0.5}La_xFe_{2-x}O_4$ spinel ferrites synthesized via co-precipitation route to evaluate structural, vibrational, electrical, optical, dielectric, and thermoelectric properties, Journal of Physics and Chemistry of Solids, 154 (2021) 110080.
[39] K.M. Batoo, G. Kumar, Y. Yang, Y. Al-Douri, M. Singh, R.B. Jotania, A. Imran, Structural, morphological and electrical properties of $Cd^{2+}$ doped $MgFe_{2-x}O_4$ ferrite nanoparticles, Journal of Alloys and Compounds, 726 (2017) 179-186.
[40] R. Sharma, S. Singhal, Structural, magnetic and electrical properties of zinc doped nickel ferrite and their application in photo catalytic degradation of methylene blue, Physica B: Condensed Matter, 414 (2013) 83-90.
[41] P. Thakur, R. Sharma, M. Kumar, S. Katyal, N. Negi, N. Thakur, V. Sharma, P. Sharma, Superparamagnetic La doped Mn–Zn nano ferrites: dependence on dopant content and crystallite size, Materials Research Express, 3 (2016) 075001.
[42] V. Lakhani, T. Pathak, N. Vasoya, K. Modi, Structural parameters and X-ray Debye temperature determination study on copper-ferrite-aluminates, Solid State Sciences, 13 (2011) 539-547.
[43] R. Sharma, P. Thakur, P. Sharma, V. Sharma, Ferrimagnetic $Ni^{2+}$ doped Mg-Zn spinel ferrite nanoparticles for high density information storage, Journal of Alloys and Compounds, 704 (2017) 7-17.
[44] A. Munajad, C. Subroto, Fourier transform infrared (FTIR) spectroscopy analysis of transformer paper in mineral oil-paper composite insulation under accelerated thermal aging, Energies, 11 (2018) 364.
[45] M.K. Raju, FT-IR studies of Cu substituted Ni-Zn ferrites for structural and vibrational investigations, Chemical Science Transactions, 4 (2015) 137-142.
[46] M. Sumalatha, S.S. kumar Reddy, M.S. Reddy, S. Sripada, M.M. Raja, C.G. Reddy, P.Y. Reddy, V.R. Reddy, Raman and in-field 57Fe Mössbauer study of cation distribution in Ga substituted cobalt ferrite ($CoFe_{2-x}Ga_xO_4$), Journal of Alloys and Compounds, 837 (2020) 155478.
[47] A. Kumar, P. Sharma, D. Varshney, Structural, vibrational and dielectric study of Ni doped spinel Co ferrites: $Co_{1-x}Ni_xFe_2O_4$ (x = 0.0, 0.5, 1.0), Ceramics International, 40 (2014) 12855-12860.
[48] P. Saxena, D. Varshney, Effect of d-block element substitution on structural and dielectric properties on iron cobaltite, Journal of Alloys and Compounds, 705 (2017) 320-326.
[49] R. Waldron, Infrared spectra of ferrites, Physical review, 99 (1955) 1727.
[50] P. Graves, C. Johnston, J. Campaniello, Raman scattering in spinel structure ferrites, Materials Research Bulletin, 23 (1988) 1651-1660.

[51] J. Massoudi, M. Smari, K. Nouri, E. Dhahri, K. Khirouni, S. Bertaina, L. Bessais, Magnetic and spectroscopic properties of Ni–Zn–Al ferrite spinel: from the nanoscale to microscale, RSC Advances, 10 (2020) 34556-34580.
[52] G. Datt, M.S. Bishwas, M.M. Raja, A. Abhyankar, Observation of magnetic anomalies in one-step solvothermally synthesized nickel–cobalt ferrite nanoparticles, Nanoscale, 8 (2016) 5200-5213.
[53] M. Abdellatif, G. Abdelrasoul, M. Salerno, I. Liakos, A. Scarpellini, S. Marras, A. Diaspro, Fractal analysis of inter-particle interaction forces in gold nanoparticle aggregates, Colloids and Surfaces A: Physicochemical and Engineering Aspects, 497 (2016) 225-232.
[54] W. White, B. Deangelis, Acid− base properties of $Cu_{1-x}Co_xFe_2O_4$ ferrospinels: FTIR investigations, Spectrochim. Acta, 25 (1967) 985-993.
[55] K. Mohit, V.R. Gupta, N. Gupta, S. Rout, Structural and microwave characterization of $Ni_{0.2}Co_xZn_{0.8-x}Fe_2O_4$ for antenna applications, Ceramics International, 40 (2014) 1575-1586.
[56] R.R. Kanna, N. Lenin, K. Sakthipandi, A.S. Kumar, Structural, optical, dielectric and magnetic studies of gadolinium-added Mn-Cu nanoferrites, Journal of Magnetism and Magnetic Materials, 453 (2018) 78-90.
[57] A.U. Rehman, N. Morley, N. Amin, M.I. Arshad, M.A. un Nabi, K. Mahmood, A. Ali, A. Aslam, A. Bibi, M.Z.Iqbal, Controllable synthesis of $La^{3+}$ doped $Zn_{0.5}Co_{0.25}Cu_{0.25}Fe_{2-x}La_xO_4$ (x = 0.0, 0.0125, 0.025, 0.0375, 0.05) nano-ferrites by sol-gel auto-combustion route, Ceramics International, 46 (2020) 29297-29308.
[58] U.B. Sontu, F. Chou, Temperature dependent and applied field strength dependent magnetic study of cobalt nickel ferrite nano particles: Synthesized by an environmentally benign method, Journal of Magnetism and Magnetic Materials, 452 (2018) 398-406.
[59] S. Thankachan, M. Kurian, D.S. Nair, S. Xavier, E. Mohammed, Effect of rare earth doping on structural, magnetic, electrical properties of magnesium ferrite and its catalytic activity, International Journal of Engineering Science and Innovative Technology (IJESIT), 3 (2014) 529-537.
[60] P. Chavan, L. Naik, P. Belavi, G. Chavan, C. Ramesha, R. Kotnala, Studies on electrical and magnetic properties of Mg-substituted nickel ferrites, Journal of Electronic Materials, 46 (2017) 188-198.
[61] T.W. Mammo, N. Murali, Y.M. Sileshi, T. Arunamani, Studies of structural, morphological, electrical, and magnetic properties of Mg-substituted Co-ferrite materials synthesized using sol-gel autocombustion method, Physica B: Condensed Matter, 523 (2017) 24-30.
[62] R.G. Kharabe, R.S. Devan, B.K. Chougale, Structural and electrical properties of Cd-substituted Li–Ni ferrites, Journal of Alloys and Compounds, 463 (2008) 67-72.
[63] V. Lakhani, K. Modi, Effect of $Al^{3+}$ substitution on the transport properties of copper ferrite, Journal of Physics D: Applied Physics, 44 (2011) 245403.
[64] M. Raghasudha, D. Ravinder, P. Veerasomaiah, Electrical resistivity studies of Cr doped Mg nano-ferrites, Materials Discovery, 2 (2015) 50-54.
[65] V. Vinayak, P.P. Khirade, S.D. Birajdar, R. Alange, K. Jadhav, Electrical and dielectrical properties of low-temperature-synthesized nanocrystalline $Mg^{2+}$ substituted cobalt spinel ferrite, Journal of Superconductivity and Novel Magnetism, 28 (2015) 3351-3356.
[66] M. Mallapur, P. Shaikh, R. Kambale, H. Jamadar, P. Mahamuni, B. Chougule, Structural and electrical properties of nanocrystalline cobalt substituted nickel zinc ferrite, Journal of alloys and compounds, 479 (2009) 797-802.
[67] R. Kambale, P. Shaikh, S. Kamble, Y. Kolekar, Effect of cobalt substitution on structural, magnetic and electric properties of nickel ferrite, Journal of alloys and compounds, 478 (2009) 599-603.
[68] M. Ajmal, A. Maqsood, Influence of zinc substitution on structural and electrical properties of $Ni_{1-x}Zn_xFe_2O_4$ ferrites, Materials Science and Engineering: B, 139 (2007) 164-170.
[69] K. Hussain, A. Bibi, F. Jabeen, N. Amin, K. Mahmood, A. Ali, M.Z. Iqbal, M.I. Arshad, Study of structural, optical, electrical and magnetic properties of $Cu^{2+}$ doped $Zn_{0.4}Co_{0.6-0.1}Fe_{1.9}O_4$ spinel ferrites, 584 (2020) 412078.
[70] C. Sujatha, K.V. Reddy, K.S. Babu, A.R. Reddy, M.B. Suresh, K. Rao, Effect of Mg substitution on electromagnetic properties of NiCuZn ferrite, Journal of Magnetism and Magnetic Materials, 340 (2013) 38-45.
[71] A.B. Mugutkar, S.K. Gore, U.B. Tumberphale, V.V. Jadhav, R.S. Mane, S.M. Patange, S.F. Shaikh, M. Ubaidullah, A.M. Al-Enizi, S.S. Jadhav, The role of $La^{3+}$ substitution in modification of the magnetic and dielectric properties of the nanocrystalline Co-Zn ferrites, Journal of Magnetism and Magnetic Materials, 502 (2020) 166490.
[72] A. Druc, A. Borhan, A. Diaconu, A. Iordan, G. Nedelcu, L. Leontie, M. Palamaru, How cobalt ions substitution changes the structure and dielectric properties of magnesium ferrite?, Ceramics International, 40 (2014) 13573-13578.
[73] G. Dascalu, T. Popescu, M. Feder, O. Caltun, Structural, electric and magnetic properties of $CoFe_{1.8}RE_{0.2}O_4$ (RE = Dy, Gd, La) bulk materials, Journal of Magnetism and Magnetic Materials, 333 (2013) 69-74.

Cover Letter

LONDON'S GLOBAL UNIVERSITY

9th December 2021

Dear Editor,

We would like to submit our manuscript entitled "**Structural, Optical, Electrical, Dielectric, Molecular Vibrational and Magnetic Properties of $La^{3+}$ doped Mg-Cd-Cu Ferrites Prepared by Co-precipitation Technique**" for publication in ***Ceramics International***.

Ferrites are among the most frequently investigated materials mainly due to interesting and practically distinguish properties. Ferrite materials have a wide range of varying properties, so correspondingly have applications over a substantial range from microwave to radio frequencies. Ferrites have low conductivity which is one of the reflections for microwave applications. Since ferrites are a significant class of magnetic materials possessing low dielectric loss factor, high resistivity, and modest to high saturation magnetization. Further tuning their structural, optical, electrical, dielectric, molecular vibrational, and magnetic characteristics by using different dopants is an important quest among the scientific community.

In present context, this work provides a unique study on a systematic effect of $La^{3+}$ compositions on $Mg_{0.5}Cd_{0.25}Cu_{0.25}Fe_{2-x}La_xO_4$ (x = 0.0, 0.0125, 0.025, 0.0375 and 0.05) ferrites. The addition of $La^{3+}$ tailored the structural, optical, electrical, dielectric, molecular vibrational, and magnetic properties. It was observed that Mg-Cd-Cu ferrites showed a larger optical band gap (2.95–3.38 eV) at room temperature, and the maximum resistivity was $7.95 \times 10^4$ Ω cm for x = 0.025. The saturation magnetization increased with the insertion of $La^{3+}$ and has a maximum value at 49.385 emu/g for x = 0.05. The calculated frequency range of $La^{3+}$ doped Mg-Cd-Cu ferrites was detected in the microwave range (3.36 – 10.80 GHz) at room temperature suggesting the potential application of the materials in longitudinal recording media and microwave absorbance.

We believe that the work is of great interest for chemists, material scientists, physicists and chemical engineers and therefore fits very well to the remit of ***Ceramics International***. Thank you very much for your consideration and we are really looking forward to hearing from you.

Yours sincerely,

Professor Nguyễn T. K. Thanh FRSC FInstP FIMMM FRSB
Chair in Nanomaterials
Vice Dean for Innovation and Enterprise, MAPS faculcy

UCL Healthcare Biomagnetic and Nanomaterials Laboratories, & Biophysics Group, Department of Physics & Astronomy, University College London, London, UK

-Editor-in-chief of the Royal Society of Chemistry book Series, Nanoscience and Nanotechnology: https://tinyurl.com/y44sybqr

-Guest Editor of Nanoscale Web themed issue on "Advanced Functional Nanomaterials for Biomedical Applications"

-Editor of the book titled "MAGNETIC NANOPARTICLES: FROM FABRICATION TO CLINICAL APPLICATIONS" CRC Press/Taylor and Francis: https://tinyurl.com/y5bgxb3r

-Editor of the book titled "CLINICAL APPLICATIONS OF MAGNETIC NANOPARTICLES" ISBN 978-1-439-86932-1 CRC Press/Taylor and Francis: https://tinyurl.com/yyjawnz2

-Co-chair of 13th International Conference on the Scientific and Clinical Applications of Magnetic Carriers, June 14-17, 2022, London, UK: http://magneticmicrosphere.com/meeting-thirteenth

Email: ntk.thanh@ucl.ac.uk, http://www.ntk-thanh.co.uk

**Declaration of interests**

☒ The authors declare that they have no known competing financial interests or personal relationships that could have appeared to influence the work reported in this paper.

☐The authors declare the following financial interests/personal relationships which may be considered as potential competing interests:

| |
|---|
| NA |

Prof. Nguyen Thi Kim Thanh